26

Jupiter's Aurora

John T. Clarke
Boston University

Denis Grodent
Universite de Liege, Belgium

Stan W. H. Cowley, Emma J. Bunce
Leicester University, England

Philippe Zarka
Ovservatoire de Meudon, Paris, France

John E. P. Connerney
NASA Goddard Space Flight Center

Takehiko Satoh
Kumamoto University, Japan

26.1 INTRODUCTION

Auroral processes are exhibited by every planet and satellite with a collisionally thick atmosphere and an internal magnetic field sufficiently strong to stand off the solar wind or plasma flow. This auroral activity is manifested as emissions produced by the impact of high-energy charged particles with the planet's upper atmosphere, with a wide range of emission brightnesses and morphologies. The aurora thereby provide a projection of magnetospheric processes, permitting the study on a global scale of otherwise invisible processes by remote sensing. For the purposes of this chapter, the definition of aurora given by Chamberlain and Hunten (1987) will be followed, in which an aurora is considered simply to be light emission produced by the impact of any external energetic particles with a planet's atmosphere.

Jupiter has by far the most energetic and brightest aurora, 100 times more energetic than the Earth's, and up to 10 times higher surface brightness. Jupiter exhibits three auroral emission regions which are physically separated from each other and vary independently, implying independent processes driving those emissions (Figure 26.1). The great energy and complexity of Jupiter's aurora stems in no small part from that planet's huge and powerful magnetosphere, which results from the strong internal field of Jupiter, the planet's rapid rotation, and the large internal source of plasma from Io. The aurora provide an enormous amount of energy deposited into Jupiter's upper atmosphere, both locally and globally. Locally, it is believed that supersonic winds at times result from the large energy input in bright auroral emission regions, where the local energy input may exceed 1 W m^{-2}(note that 1 mW m^{-2} =1 erg $(cm^2\ s)^{-1}$). Globally, the auroral energy input of up to 10^{14} W exceeds the solar UV flux absorbed by the upper atmosphere across the planet by a factor of 20–50, depending upon solar activity. In this sense, the global upper atmosphere of Jupiter is energetically driven by the aurora rather than by absorbed sunlight, as is the case on the Earth. This refers to the solar UV flux absorbed in the upper atmosphere: the visible solar flux which penetrates to lower altitudes exceeds these amounts by orders of magnitude.

There is a long and colorful history to the observations of Jupiter's aurora, extending back to the 1950s when nonthermal radio emissions were detected, and the late 1970s when the UV aurora were first observed. Understanding of the aurora has steadily increased as a result of improved observational platforms and the discovery of new emissions at various wavelengths. This chapter first presents a general discussion of Jupiter's aurora in Section 26.1, including an historical overview of auroral observations and issues relating to their interpretation, comparison with the Earth's auroral processes, a summary of early theoretical ideas about Jupiter's auroral processes, and attempted correlations of the auroral intensity with solar wind properties. This is followed by more specific discussions of the physical processes in the three auroral regions in Sections 26.2.4.

26.1.1 Observations of Jupiter's Auroral Emissions and Magnetospheric Processes

There have been literally hundreds of papers and meeting abstracts published on multi-wavelength observations of

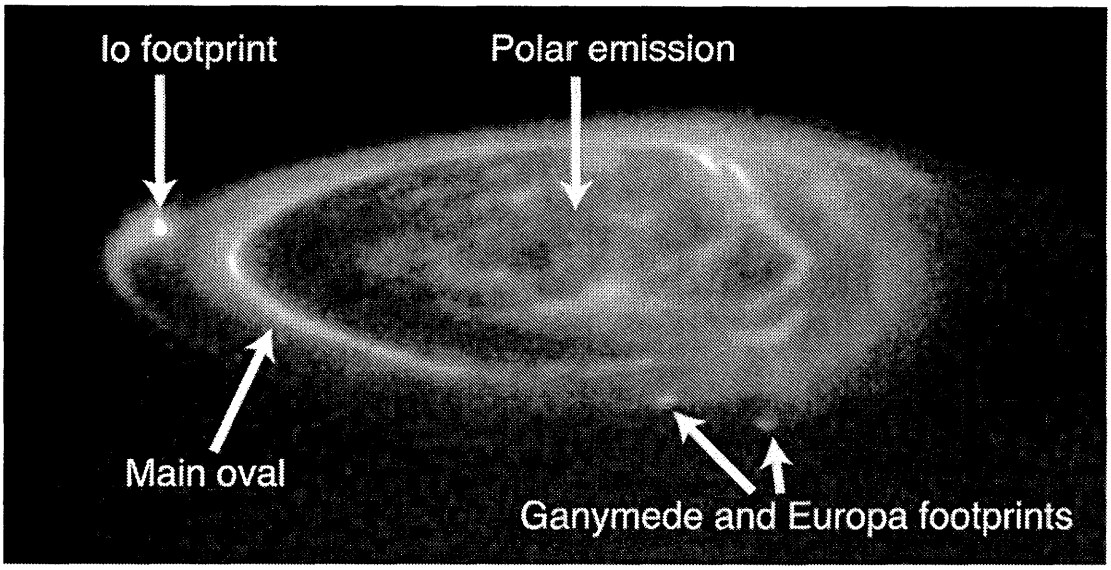

Figure 26.1. HST STIS UV image of Jupiter's northern aurora taken in November 1998, showing the 3 different emission regions: the main oval, the satellite footprints, and the polar emissions. The image has been scaled with a logarithmic stretch in intensity to make clear the faint emissions next to brighter ones. Note the resolved auroral curtain above the limb, particularly in Io's magnetic footprint. At the time of going to press a colour version of this figure was available for download from http://www.cambridge.org/9780521035453.

Jupiter's aurora. In this short section only the highlights are presented. More detailed information can be found in recent review papers (Zarka 1998, Bhardwaj and Gladstone 2000, Waite *et al.* 2000, Bhardwaj, Gladstone, and Zarka 2001, Clarke 2003). This section presents in historical order the discovery of Jupiter's auroral emissions and related processes, including non-thermal radio emissions, with details of the emission processes provided as each topic arises. Some specific topics leading to our present understanding of auroral processes are then presented.

It has been known since the 1950s that Jupiter is an intense source of non-thermal radio emissions (Burke and Franklin 1955), implying the presence of a strong magnetic field. Jovian radio emissions were detected from frequencies near the Earth's ionospheric cut-off (~10 MHz) up to 40 MHz, and were soon attributed to cyclotron emission of gyrating electrons. Interpreting the highest detected frequency as an electron gyrofrequency gave an early estimate of the maximum field strength up to 14 gauss, close to the presently known value. The subsequent discovery that the jovian decametric (DAM) radio emissions were modulated by the orbital location of Io (Bigg 1964) indicated that Jupiter had an electromagnetic interaction with the innermost Galilean satellite. The first spacecraft visits provided many details about the jovian system. Jupiter's ionosphere was first detected by radio occultation during the *Pioneer 10* flyby in 1974 (Kliore *et al.* 1974), and ground-based telescopic observations first detected the plasma torus in the mid 1970s (Brown 1976). The first in situ measurements of the jovian magnetosphere were conducted during the *Pioneer* and *Voyager* encounters, and it was during the *Voyager 1* flyby in 1979 that Jupiter's aurora was first detected (Broadfoot *et al.* 1979) by observations at UV wavelengths.

26.1.2 Radio Emissions and Generation Mechanisms

During their flybys of Jupiter in 1979, the *Voyager 1* and *2* spacecraft considerably extended our knowledge of jovian radio emissions, especially the low frequency components: hectometric (HOM) emissions are observed in the band from ~200 kHz to a few MHz, broadband kilometric emissions (bKOM) from ~10 kHz to <1 MHz, and narrowband kilometric emisions (nKOM) in the range 100–200 kHz (Carr *et al.* 1983 and Figures 26.2 and 26.4). The radio astronomy experiments aboard these spacecraft also detected ubiquitous radio emissions at Saturn, Uranus and Neptune (Zarka 1998). Observations by the *Ulysses* spacecraft during its flyby of Jupiter in 1992 demonstrated the high-latitude origin of HOM and bKOM (Ladreiter *et al.* 1994), while the nKOM was found to be radiated at the local plasma frequency (f_{pe}) by localized sources in Io's torus (Reiner *et al.* 1993) (Figure 26.3). Quasi-periodic radio bursts (QP) occurring at intervals of 15 to 40 minutes were also identified by *Ulysses*, with a possible auroral origin (MacDowall *et al.* 1993). Further observations by *Wind*, *Galileo* and *Cassini* improved our understanding of the generation of radio emissions and their variability. It is now well established that auroral jovian radio components are coherent non-thermal radiations produced by an instability near the local electron cyclotron frequency (f_{ce}) in high magnetic latitude regions. This so-called "cyclotron maser" instability requires the presence of out-of-equilibrium electron populations with a characteristic energy of a few keV in an intense magnetic field (where $f_{pe} \ll f_{ce}$). These conditions are fulfilled in the jovian high latitude regions (auroral regions and vicinity of the Io flux tube footprints).

Jovian non-thermal radio emissions extend from the kilometer to the decameter range, auroral radio emissions, including the non-Io-DAM, HOM, bKOM, and perhaps QP components. They share the following common properties:

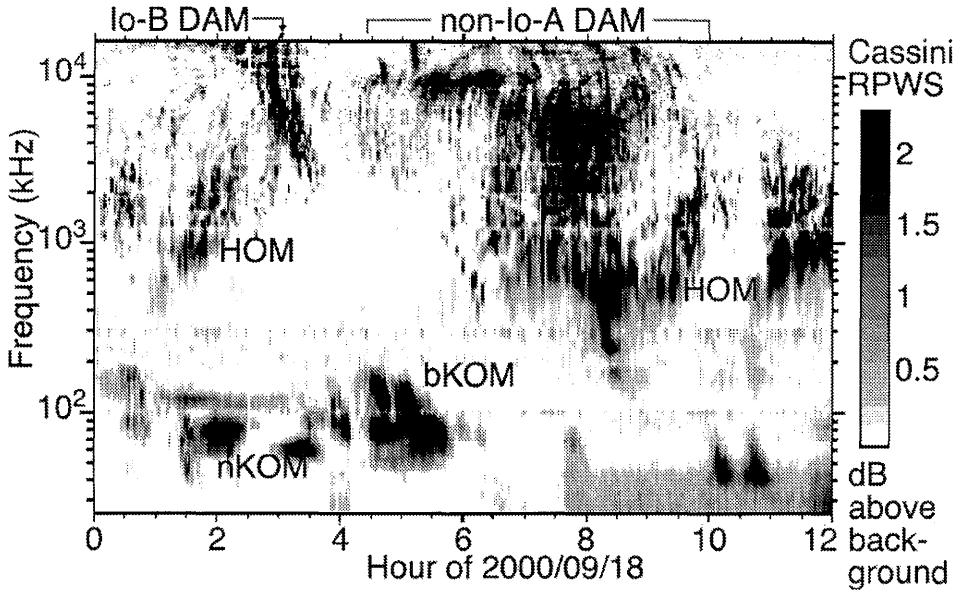

Figure 26.2. Jovian low-frequency radio emissions detected on 18 September 2000 by the RPWS (Radio and Plasma Waves Science) experiment onboard *Cassini* approaching Jupiter. The Io-DAM emission (labeled "Io-B DAM") appears here down to about 2 MHz, while Io-independent emission ("non-Io-A DAM") merges with the hectometer component ("HOM") detected down to 200–300 kHz. The auroral broadband kilometer component ("bKOM") is detected down to ~40 kHz. The narrowband emission ("nKOM") is generated at or near the plasma frequency f_{pe} in Io's torus. Adapted from Figure 1 of Zarka *et al.* (2001a).

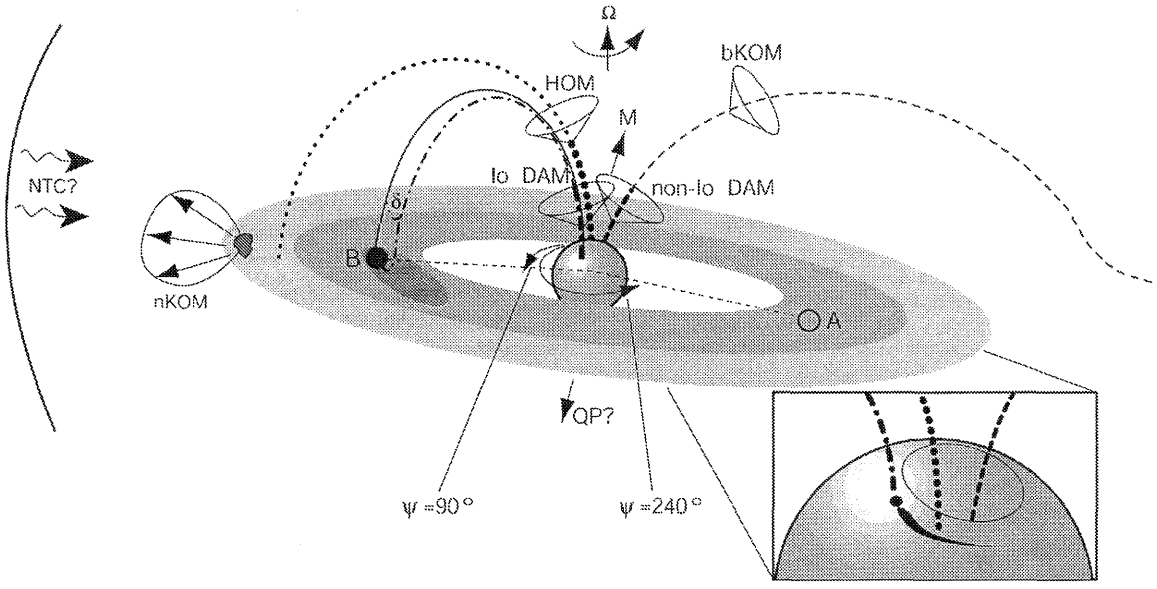

Figure 26.3. Sketch of radio source locations in the jovian magnetosphere. Boldface cones emphasize high latitude emission sources, which actually exist in both hemispheres. bKOM, HOM and DAM are generated near the local electron gyrofrequency f_{ce} and beamed in widely opened hollow cones aligned on magnetic field lines with $L \sim 6$ (Io-DAM), $L = 7$–9 (HOM), $L > 10$ (bKOM), and $L \geq 7$ (non-Io-DAM) (Ladreiter *et al.* 1994, Zarka *et al.* 2001a). The inset shows the correspondence of these radio sources with UV ones (main oval with non-Io DAM and bKOM, and Io's spots and trail with Io-DAM). QP may originate – at least in part – from southern auroral latitudes, while NTC was thought to be produced at density gradients near the magnetopause (Kurth 1992), or alternately may be the low frequency end of QP bursts having been reflected on magnetospheric density gradients. nKOM is emitted in broad beams by unidentified torus inhomogeneities. Adapted from Figure 3 of Zarka (2000).

(1) They are extremely intense (brightness temperature $T_b > 10^{15}$ K). (2) They are emitted at a frequency close to the X mode cut-off, itself close to the local electron cyclotron frequency $f \sim f_X \sim f_{ce}$, from high magnetic latitude northern and southern sources where $f_{pe}/f_{ce} \ll 1$. (3) They are 100% circularly or elliptically polarized. (4) They are beamed at large angles from the magnetic field in the source region. These properties are quite similar to those of Earth's auroral kilometric radiation (AKR). They imply a non-thermal, coherent generation mechanism of high efficiency,

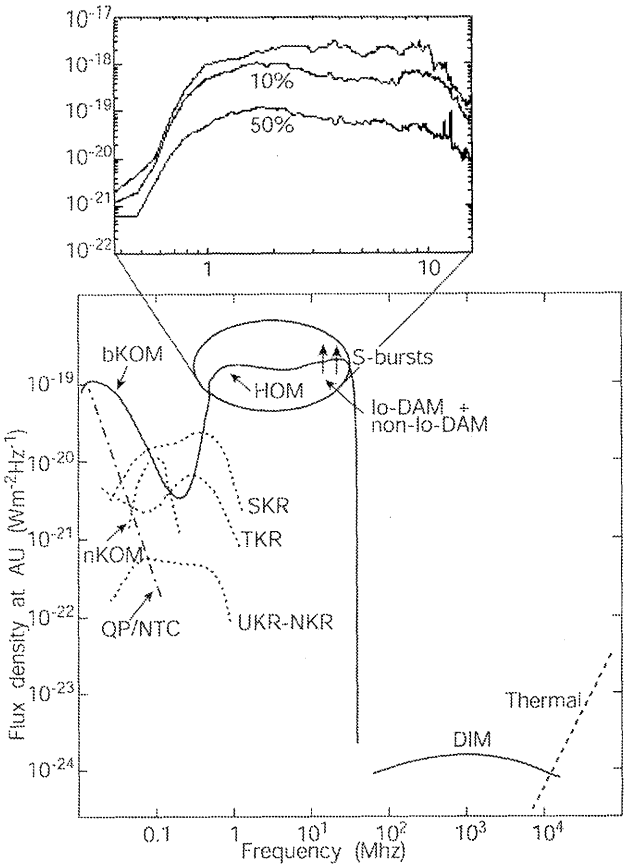

Figure 26.4. Lower panel: Spectra of all jovian radio components, including the thermal and synchrotron (DIM) components, and auroral radio emissions from the other radio planets: (T)errestrial/(S)aturn/(U)ranus/(N)eptune Kilometric Radiation. Boldface lines emphasize jovian high-latitude emission spectra. Part of Io-DAM consists of impulsive "S"-bursts ("S" = short). QP bursts seem to merge at low frequencies to form the non-thermal continuum (NTC) that escapes the magnetosphere (Kaiser 1998). Frequencies $\geq$10 MHz are observable from the ground. The spectra below 40 MHz were computed from *Voyager* PRA measurements (Warwick *et al.* 1977). Upper panel: Typical spectra of jovian HOM/DAM emissions recorded by *Cassini*-RPWS, corresponding to the levels observed 1%, 10%, and 50% of the time. They illustrate the $>\times 10$ sporadicity of the emission over periods of a few hours. Adapted from Figure 2 of Zarka (2000).

identified as the cyclotron maser instability (CMI), in which gyrating energetic electrons can resonantly amplify RH-X mode waves at the expense of their perpendicular energy (Louarn 1992, Zarka 1998 and references therein).

According to the CMI, energetic electrons gyrating at a circular frequency ω_{ce}/Γ can remain temporarily in phase resonance with the electric field of RH-X mode waves with Doppler-shifted frequency ω–$k_{||}v_{||}$ (in the electron's frame), leading to perpendicular energy transfer and thus direct wave amplification or attenuation and electron diffusion in velocity space ($v_{||}$,$v_{\perp}$). If the electron velocity distribution $f(v_{||},v_{\perp})$ contains free energy, wave growth becomes possible (see Zarka 1998 and references therein).

Differences in the CMI operation at Jupiter and at Earth may arise from Jupiter's rapid rotation and strong magnetic field. This may lead to large-scale depleted radio sources and saturated DAM emission, and to the possibility of Io's torus quenching the mechanism at HOM frequencies along field lines traversing it.

26.1.3 Early Auroral Observations

The first detection of the aurora was by the *Voyager 1* UVS during its Jupiter encounter in spring 1979, followed within a couple of months by observations from the International Ultraviolet Explorer (IUE) from Earth orbit. The UV auroral emissions closely resemble the laboratory spectrum of electron collisional excitation of H_2. The most prominent emissions are the H_2 Lyman ($B^1\sum_u^+ - X^1\sum_g^+$) and Werner ($C^1\prod_u - X^1\sum_g^+$) band series plus the H Lyα line (Figure 26.5). Additional UV auroral emissions result from fast proton and H atom collisional excitation. During the *Voyager 1* and *2* encounters (Sandel *et al.* 1979) the long aperture of the UVS was used to map the equatorward extent of the UV auroral emissions. These maps indicated that auroral emissions first appeared when the end of the aperture covered the expected latitude of the magnetic mapping of the plasma torus into Jupiter's atmosphere, seemingly implicating the plasma torus as the source of auroral particles.

The IUE observations (Clarke *et al.* 1980, Skinner *et al.* 1984, Livengood *et al.* 1992, Harris *et al.* 1996, Prangé *et al.* 2001) provided much more extensive information on the spatial and temporal variations of the UV aurora from Jupiter's north and south polar regions. The IUE spectra confirmed the identification of Jupiter's auroral emissions as produced by electron collisional excitation of H_2 and H in the jovian atmosphere (Waite *et al.* 1983), at 1.0 nm resolution compared with the *Voyager* UVS 3.0 nm resolution. Further observations with the Hopkins Ultraviolet Telescope (HUT) (Wolfven and Feldman 1998, Morrissey *et al.* 1997) and *Galileo* UVS (Ajello *et al.* 1998) provided independent measurements of the auroral spectrum. IUE studies first showed that the auroral emission regions rotate with Jupiter's magnetic period (System III), in contrast with the Earth's aurora which remains fixed with the direction of the solar wind. They also showed that Jupiter's aurora are essentially always active but exhibit variations from day to day, although the variability rarely exceeds a factor of two in total auroral emission brightness and therefore power. The IUE spectra first inspired the definition of the auroral "color ratio" (CR), which is the ratio of wavelength bandpasses where there is strong hydrocarbon absorption to a band where there is little absorption (Yung *et al.* 1982). The strength of the absorption indicates the depth of penetration of the precipitating charged particles, and can be related to their incident energy, taking advantage of the rapid decrease in hydrocarbon densities with altitude above the homopause level where molecular diffusion dominates. Detailed modeling of the collisional loss of energy of incident charged particles with Jupiter's auroral atmosphere and the subsequent radiative transfer of the emissions leaving the atmosphere (Rego *et al.* 1999a, Grodent *et al.* 2001) has provided some rules of thumb. To a good approximation, 100 kR emission (1 kRayleigh = 10^9 photons/second from a 1 cm^2 column of the atmosphere radiated into 4π steradians) corresponds to an input power of 10 mW m^{-2}. The color ratio (CR) as a

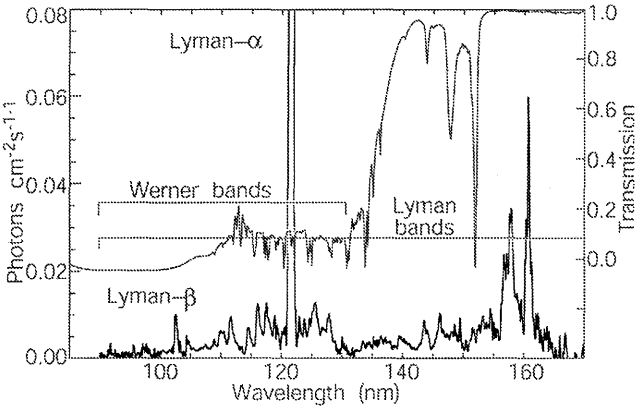

Figure 26.5. Jupiter's UV auroral emission spectrum from Hopkins Ultraviolet Telescope (HUT) observations (Morrissey *et al.* 1997), with principle emission bands of H_2 and H indicated. The atmospheric transmission spectrum for a typical main oval aurora is indicated with the light, upper line.

function of the mean electron energy for a Maxwellian distribution of primary electrons at the top of the atmosphere and a view angle of 60° is:

CR ~ 1, <E> ≤ 10 keV (unabsorbed value)

CR ~ 2, <E> = 60 keV (medium absorption, typical for main oval)

CR ~ 4, <E> = 100 keV (strong absorption, dawn storms and some polar emissions)

where <E> is the mean electron energy, that is twice the characteristic energy of the Maxwellian distribution. The color ratio = I(155–162 nm)/I(123–130 nm), where I is given in photon units. IUE studies gave values of CR = 1.5–2, corresponding to input electrons of 30–40 keV, and showed a systematic variation in color ratio with longitude, with the maximum CR appearing in the north in images taken near System III central meridian longitude λ_{III} CML ~ 180°. Higher resolution spectra obtained with the HST GHRS instrument later provided measurements of the ro-vibrational H_2 temperature in the emitting region, indicating the neutral heating at auroral altitudes (Trafton *et al.* 1994, Clarke *et al.* 1994, Kim *et al.* 1995, Liu and Dalgarno 1996).

26.1.4 Near-IR Aurora

An early mystery about Jupiter's auroral upper atmosphere was the fate of the large amounts of collisionally induced heating that must accompany the emissions. Jupiter's upper atmosphere has few molecules which can effectively radiate heat, being composed mainly of H_2, He, and H. While hydrocarbons can radiate strongly in the IR, their abundances at the altitude of the auroral curtain are insufficient to prevent the temperature from reaching much higher values than were measured. This mystery was partially solved when observations were performed in the late 1980s to detect quadrupole emissions from H_2 near 2.1 microns, where dipole-allowed transitions of H_2 produce strong absorption of reflected sunlight. The detection of more than a dozen lines in addition to the expected H_2 lines, previously unidentified outside of the laboratory, led to the discovery of near-IR thermal emissions from ro-vibrational transitions of H_3^+ in Jupiter's auroral ionosphere (Drossart *et al.* 1989, Trafton *et al.* 1989). These emissions radiatively cool the auroral thermosphere at the rate of ~1 mW m^{-2}, and have since been used for imaging and spectroscopic studies of Jupiter's aurora from ground-based telescopes (Kim *et al.* 1991, Baron *et al.* 1991, Kim *et al.* 1994, Connerney *et al.* 1996, Stallard *et al.* 2002). H_3^+ is formed in the jovian ionosphere by the rapid ion–molecule reaction which follows ionization of molecular H_2:

$$H_2 + h\nu\ (\lambda < 80.4\ nm) \rightarrow H_2^+ + e^-$$
$$H_2^+ + H_2 \rightarrow H_3^+ + H$$

H_3^+ is the major ionospheric ion from 1 to 100 microbars (Kim and Fox 1994, Achilleos *et al.* 1998). The IR emissions are thermal emissions, rather than being directly excited like the UV emissions, so that their intensity is proportional to the number density and fourth power of the temperature. One implication of this fact is that if the incoming flux of electrons were to be suddenly cut off, the UV emissions would disappear in a small fraction of a second while the H_3^+ emissions would decay with a 1/e lifetime of the order of 100–1000 s from theoretical estimates. An experiment to determine this rate from the time variations of observed H_3^+ emissions gave a decay time of ~10 min (Satoh and Connerney 1999). In this sense, the H_3^+ aurora are analogous to an oscilloscope screen with the decay time set to a long interval. It also means that the H_3^+ aurora can show energy inputs integrated over extended times, and reveal energy transferred from the active precipitation regions, for example into the ionosphere poleward of the main oval where there may be no active precipitation. They may also result from ionospheric heating by low energy electrons, for example by ionospheric currents. H_3^+ emissions have also been used to measure Doppler motions of ions in the auroral electrojet (Stallard *et al.* 2001, see Chapter 9).

26.1.5 Comparison of UV and IR Aurora

While the H_3^+ emissions are known to exhibit a similar morphology to the UV emissions, no detailed comparison has previously been published. In this chapter, the first direct comparison of nearly simultaneous UV and IR images of Jupiter's aurora is presented, obtained on 16 December 2000 (Figure 26.6). In this figure, the initial images are first presented, then a comparison is made after similar processing of the two images. The IR images are normally corrected for limb brightening, then deconvolved. For a direct comparison, the UV image has first been blurred to the resolution of the initial IR image, then deconvolved with the same algorithm as the H_3^+ image. The resulting appearance of the aurora is similar in the two wavelengths, although there are significant differences. The IR image still appears more limb brightened than the UV image, even after correction for a cosine-function limb brightening. Simulations of the appearance of the auroral curtain on Jupiter have shown that this is the result of the high transmissivity of the jovian atmosphere at the altitude of the H_3^+ missions to IR wavelengths. Simulated auroral images appear strongly limb brightened until the UV absorption up to the homopause level is included, then the images look much like the initial UV image. The strong difference in limb brightening is attributed to the altitude from the peak of the auroral curtain down to the height where the transverse atmosphere is optically thick. This difference in altitude is ~50 km in the UV and ~350 km in the IR.

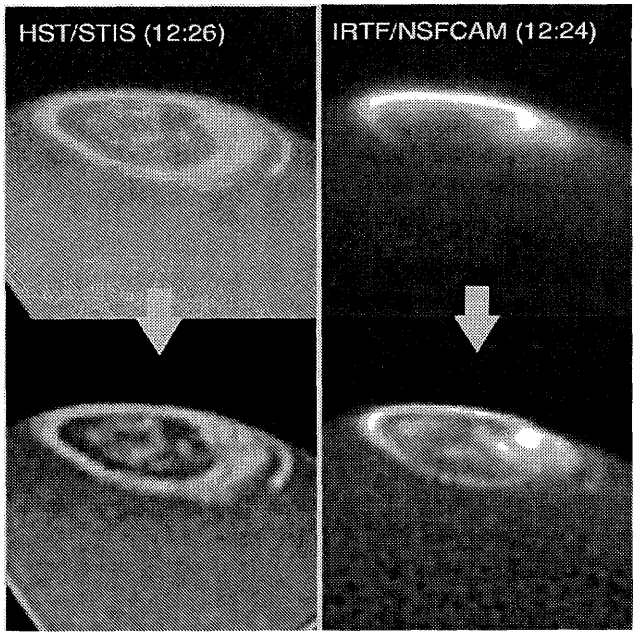

Figure 26.6. Comparison of UV and H_3^+ IR images of Jupiter's aurora taken 2 min apart on 16 December 2000. The upper panels show the UV (left) and IR (right) images after standard reduction, before any additional processing. The lower panels show the same images after deconvolution and correction for limb brightening (IR – right) and blurring to the IR resolution followed by the same deconvolution (UV – left). The IR image has also been corrected for limb brightening. The differences in appearance of the IR and UV images are discussed in the text. At the time of going to press a colour version of this figure was available for download from http://www.cambridge.org/9780521035453.

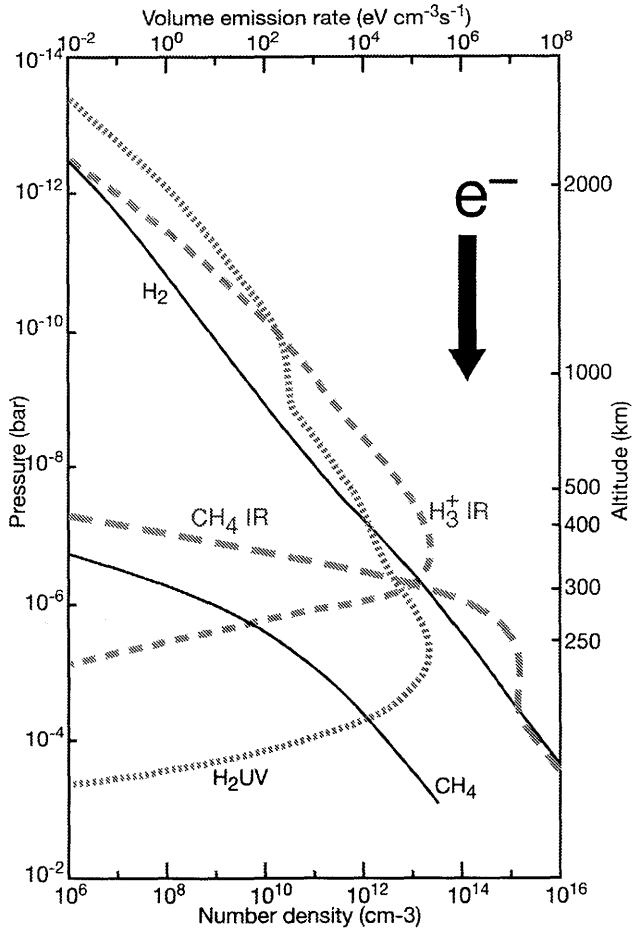

Figure 26.7. Plot indicating models for the altitude production rates of various auroral emissions described in the chapter. Solid lines indicate number densities, and dashed lines indicate volume emission rates. The profiles are from the model of Grodent *et al.* (2001), in which the collisional degradation of incoming electrons is treated, and heating and radiation processes are calculated. The model is constrained by the measured atmospheric structure extended to auroral latitudes, and the observed UV color ratio of the main oval.

After the IR image has been corrected for limb brightening, the most pronounced single feature is the bright emission on the right-hand side of the main oval, which does not appear in the UV image. This feature may imply strong auroral activity over a preceding interval, which might appear in the more slowly-varying H_3^+ but not in the UV, or it might be a real transient feature in the aurora which had faded by the time of the UV image. As stated earlier, it could also imply ionospheric heating. Discrete features along the main oval in the UV image also are not clearly discerned in the H_3^+ image. Emissions from the magnetic footprint of Io and its trail appear in both wavelength bands, however, the UV intensity is comparable to that of the main oval while the IR intensity is lower than most of the main oval. The diffuse emissions just to the left of the Io footprint and equatorward of the main oval also appear in the UV but not in the IR. The polar emissions also appear different in the two images, but these are known to vary on timescales less than the 2 minute separation of the images.

26.1.6 X-ray and Thermal IR Aurora

Jupiter also emits strong X-ray emissions (Metzger *et al.* 1983, Waite *et al.* 1994) which have a different morphology than the other aurora, with emissions concentrated in the polar regions and extending to low latitudes with a greatly reduced intensity. These emissions were initially interpreted as K shell lines of O and S, representing a population of high energy precipitating ions presumably originating at Io. The most recent high resolution images from the Chandra X-ray telescope have shown the X-rays to be concentrated in the same region as the polar flares (Section 26.1.9) first observed in UV images (Gladstone *et al.* 2002, and see Section 26.4.1), and also suggest that the X-rays might be produced by electron bremsstrahlung. A more detailed discussion of the X-ray aurora is given by Bhardwaj and Gladstone (2000). Thermal IR observations (Caldwell *et al.* 1980, Drossart *et al.* 1986, Caldwell *et al.* 1988, Kostiuk *et al.* 1993, Livengood *et al.* 1993, Kim *et al.* 1993) have also recorded auroral emissions from hydrocarbon molecules over a range of altitudes near and below the homopause. These emissions arise in Jupiter's upper stratosphere, with a maximum in the contribution function well below the UV and visible auroral curtains, and they are brightest in a "hot spot" which appears coincident with the UV flares and X-ray active region. They provide further information on the heating and photochemistry of the auroral atmosphere, but are as yet relatively poorly understood in terms of the populations and photochemistry leading to the emissions. A comparison

of the altitude profiles of the auroral emissions at different wavelengths based on a model for the auroral energy deposition is given in Figure 26.7. It can be seen that the H_3^+ emissions are produced highest in the atmosphere, the UV emissions somewhat lower (but with a large vertical extent), and the thermal IR emissions peaking lower still.

26.1.7 HST UV Images

A new era opened when high resolution ultraviolet images became available with the Hubble Space Telescope (HST), first with the Faint Object Camera (FOC) (Caldwell *et al.* 1992, Gérard *et al.* 1994a, Prangé *et al.* 1998), and later with the Wide Field and Planetary Camera 2 (WFPC2) (Clarke *et al.* 1996, Ballester *et al.* 1996, Morrissey *et al.* 1997, Clarke *et al.* 1998). These instruments obtained the first high resolution images of the complex jovian auroral morphology. The FOC images, with a limiting sensitivity of 50–100 kR, are noteworthy for being the first to identify the high latitude of the main oval. This suggested the mapping to a distance of the order of 30 R_J by comparison with the O6 magnetic field model. Improved estimates as outlined below now indicate that the mapping is better estimated at 20–25 R_J. The FOC images also indicated an asymmetry between the dawn and dusk sides of the northern aurora, with a narrow arc on the morning side and much more diffuse emissions on the afternoon side (Gérard *et al.* 1994a). Much of this asymmetry is now known to be fixed in Jupiter's magnetic field and rotating with the planet. At least one FOC image also showed the location of the Io footprint in the southern aurora (Prangé *et al.* 1996), although this feature was not consistently detected in the FOC images due to limited sensitivity.

The WFPC2 images, with a limiting sensitivity of 10 kR, showed much more of the full distribution of the emissions. This is also the only camera on HST which has imaged both poles in the same frame. The Io footprints are consistently detected in these images, providing accurate locations (along with H_3^+ images) for the creation of the VIP4 magnetic field model (Connerney *et al.* 1998). The VIP4 model is based on in situ measurements from the *Voyager* and *Pioneer* magnetometers plus the observed latitudes of the Io footprints from both HST and H_3^+ images. Lead angles and brightnesses of the Io footprint emissions have also been measured. A high degree of conjugacy was found between the northern and southern emissions in the main oval within the limits of the observing geometry, and individual emission features were found to corotate with the planetary magnetic field. No emissions have been detected equatorward of the locus of Io footprints, setting a limit of the order of 0.1 mW m^{-2} to the energy of any auroral processes in the inner magnetosphere. Bright emissions (>10 MR) fixed near magnetic local dawn (the "dawn storms") have been observed by all 3 cameras on HST (see Section 26.3), and these were established to occur along the main oval in WFPC2 images. The separate emission regions (main oval, footprints, and polar emissions) and the timescales for their variations up to a few × 100 s are clearly seen in the WFPC2 images. WFPC2 UV imaging provided the main auroral observations during the impacts of Comet Shoemaker–Levy 9 in 1994 (Clarke *et al.* 1995, Prangé *et al.* 1995). These include the detection of northern auroral emissions conjugate to the impact and ejection plume "splashdown" sites in the south (Bauske *et al.* 1999), interpreted as driven by an ionospheric dynamo action resulting from the initial impact and splashdown (Hill and Dessler 1995).

Much greater detail on Jupiter's UV auroral emissions became available with the Space Telescope Imaging Spectrograph (STIS) on HST, which provided the detection of new auroral features with an order of magnitude higher sensitivity than earlier cameras. Its higher resolution and sensitivity to ~1 kR emissions allows the tracking of local time features and time resolution on the brightness of transient features (Waite *et al.* 2001, Clarke *et al.* 2002a). STIS images also provide a much more detailed view of the diffuse emissions both equatorward and poleward of the main oval than was possible with the FOC and WFPC2. The images revealed a long, persistent trail of emission extending from the Io footprints, in the direction corresponding to the plasma flow direction downstream of Io. At times there has also appeared a second emission peak downstream, with a brightness up to the level of the primary emission feature. These emissions provide important tests of theories of plasma pickup near Io. The STIS observations also detected auroral emissions from the magnetic footprints of Europa and Ganymede. These always appear on the equatorward side of the main oval, which unambiguously requires the majority of the auroral emissions to map to distances greater than the orbital distance of Ganymede, or 15–20 R_J (Clarke *et al.* 2002a). Combined with the observations of near-corotation of observed emission features, this demonstrated the mapping of the main oval to ~20–25 R_J, which is the region where corotation breaks down in the outward drifting plasma. It is significant that the distance to which the main oval maps was determined by imaging the aurora, rather than in situ measurements of the plasma or currents.

A detailed analysis of a series of STIS images obtained as *Cassini* approached Jupiter (Grodent *et al.* 2003a) revealed several systematic trends in the aurora. New "reference" oval locations were defined based on the sums of images in the north and south, and the overall auroral morphology was shown to be fixed in jovian System III coordinates over at least 5 years time. The main oval was found to contract slightly near local noon, and to contract with an overall brightening on one day, apparently correlated with increased solar wind pressure. Comparison of auroral images with *Cassini* and *Galileo* measurements provided evidence of diffuse emissions mapping to the instantaneous position of *Galileo* at ~15 R_J where the *Galileo* EPD instrument detected plasma injection events (Mauk *et al.* 2002). This is the first case of simultaneous auroral imaging and measurement of the responsible precipitating particles on a planet other than the Earth. Simultaneous images at UV and X-ray wavelengths (Gladstone *et al.* 2002) showed that strong X-ray emissions are produced in the "active region" where UV flares are also observed.

26.1.8 *Galileo* Visible Images

The highest resolution images of Jupiter's aurora taken to date have been obtained from the visible camera on the *Galileo* spacecraft (Ingersoll *et al.* 1998, Vasavada *et al.* 1999). These images have only been obtained of the nightside of Jupiter, and must be carefully planned in line of sight

and exposure time to avoid scattered light from the sunlit atmosphere. They have shown the structure of the auroral curtains at a scale down to 26 km/pixel, although over limited areas of the auroral zones and with limited dynamic range, and shown the location and morphology of the brighter emissions on the nightside of the planet. The visible wavelength aurora are produced by the same collisional excitation as the UV emissions, and result from relatively lower energy electronic transitions in H_2 and H. In this sense they are also prompt emissions sensitive to the degradation in energy of the primary particles. Images of the auroral curtain above the planet limb show that the height of the base of the curtain is 245 ± 30 km above the 1 bar level. They also show that the width of the main oval, while variable with location and time, is typically a few hundred km. The auroral morphology on the nightside is similar to that on the dayside, with some important distinctions which will be discussed in more detail in Section 26.3. Discrete emissions have been reported which resemble satellite footprints, however the images also show lightning storms at similar latitudes as the satellite footprint locations, leading to an ambiguity. The reported locations of the Io footprint from visible images where these can be clearly identified give similar locations as in the UV and H_3^+ images. It has been shown that the distorted main oval shape in the north around λ_{III} = 140–180° also appears on the nightside, indicating it is fixed with Jupiter rather than in local time.

26.1.9 Interpreting Observations of Jupiter's Aurora

Overall, Jupiter's UV aurora exhibit main emission ovals which are aligned about the north and south magnetic poles and corotate with the planet at the System III (magnetic) rotation period, in contrast with the Earth's auroral pattern which remains fixed with respect to the solar wind direction. In addition to this general pattern, there are pronounced variations of Jupiter's auroral emission along these ovals, and there are significant motions of the emissions with respect to the time-averaged oval locations. In addition to the main ovals, there are more variable emissions observed poleward of the main ovals and localized emissions associated with the satellite Io, which have been identified with Io through their persistent appearance near the expected locations of Io's magnetic footprints. The polar emissions map along Jupiter's magnetic field to greater distances in the magnetosphere, but the open field line region is not known with any great certainty. For this reason we refer to emissions poleward of the main oval simply as "polar" emissions, rather than "polar cap", which refers to regions along open field lines at the Earth.

The appearance of Jupiter's aurora may vary greatly depending on the properties of the instrument used to make the images. To illustrate this point, a comparison of the imaging resolution obtained with various UV instruments is shown in Figure 26.8. Each of these images is of the northern aurora near 180° central meridian longitude (CML), and presented with a log stretch in intensity to enhance the fainter emissions. They are all presented with the "pipeline" processing and background subtraction for an equal comparison. For the IUE panel, the WFPC2 image has been smoothed to 5 arcsec resolution to simulate the IUE angular resolution within the large aperture (marked with lines). A more detailed comparison of the imaging properties of the 3 cameras on HST is given by Clarke (2003). Note that the angular resolution is limited by the instrumental resolution and, in the case of planets, also by the exposure time due to rotational blurring. For Jupiter's rotation of ~1° longitude $(100\ s)^{-1}$, the HST camera resolutions of the order of 0.05–0.1 arcsec can only be preserved in exposures less than about 100 s. In this case, spatial resolutions on the order of 300 km can be achieved. Short exposures require high sensitivity, therefore high instrumental throughput is needed for higher angular resolution. Another important element of the images is the ability to assign absolute longitude/latitude positions to observed emissions. Uncertainties for FOC and STIS, where only part of the planet disc is imaged in the field of view, are several pixels or ~0.1 arcsec or ~400 km projected distance, while the WFPC2 images with the whole disc can be somewhat more accurate. For observations of Io's footprint, as Jupiter rotates, Io moves through different regions of the magnetic field. The rapidly changing declination of the field at Io directs the footprint to locations which can vary rapidly east/west on Jupiter (by ± 40° from the sub-Io longitude in the north), rather than moving slowly in local time. This introduces an added blurring in images of footprint emissions, and must be estimated for each image.

Of the three distinct auroral regions, the satellite footprint aurora are readily identified by the fact that they remain fixed along magnetic flux tubes connected to Io, Europa, and Ganymede (Clarke *et al.* 2002a). The main oval emissions are observed to corotate with Jupiter (Ballester *et al.* 1996), and are relatively stable, exhibiting variations on timescales of tens of minutes to hours. By contrast, the polar emissions vary rapidly, with no correlation seen between these variations and the main oval or footprint brightnesses. The extreme cases are called polar "flares" (Waite *et al.* 2001), which can rise from the background level of a few kR to several MR brightness in tens of seconds. The three regions are therefore regarded as representing separate auroral processes from different regions in the magnetosphere. This is consistent with the association of the satellite footprints with standing current systems from the satellites, and the main oval with upward Birkeland currents from the region of the current sheet where plasma corotation breaks down. Further subdivisions may result in time upon closer examination of the polar region emissions. The second half of this chapter is divided by emission region for more detailed discussions of the processes driving these three auroral types.

The energetic processes producing Jupiter's auroral emissions also deposit large amounts of energy into the upper atmosphere, and estimated powers in the different auroral regions provide key information about the nature of magnetospheric processes leading to the emissions. For the UV and visible emissions, approximately 10% of the input power is converted to radiation (the exact value depends on the energy of the precipitating particles, Waite *et al.* 1983, Grodent *et al.* 2001), so that the observed radiated energy can be multiplied by 10 for a rough estimate of the total energy input. The energy input to the upper atmosphere is mainly in the form of heat, plus ionization and dissociation (mainly of H_2). The overall power input to Jupiter's aurora from the integrated emissions is estimated to be up to 10^{14}

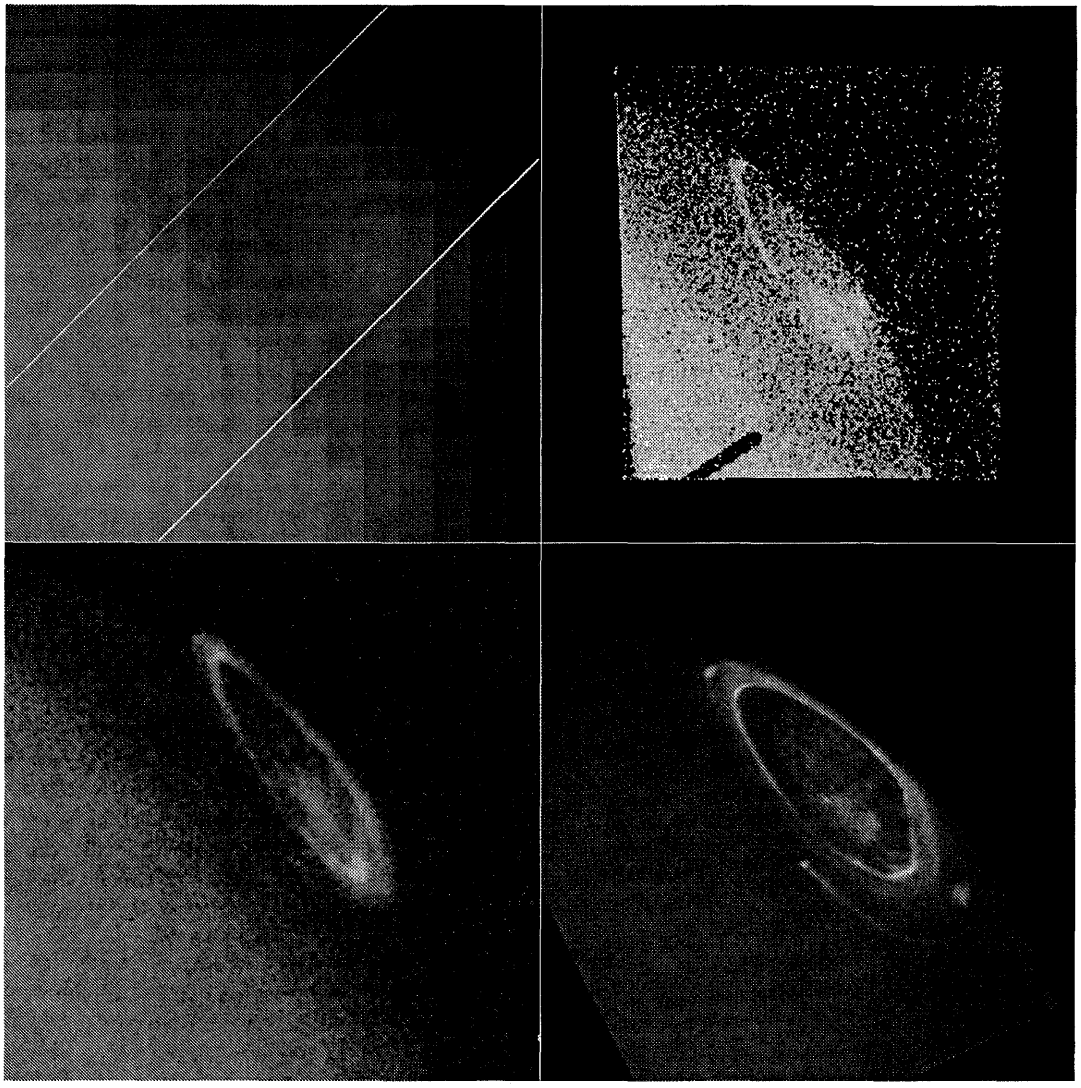

Figure 26.8. Comparison of UV images of Jupiter's aurora from IUE (simulated, upper left), HST post-COSTAR FOC (upper right, 716 s), HST WFPC2 (lower left, 500 s), and HST STIS (lower right, 120 s). Each of these images is of the northern aurora near 180° CML, and they are presented with the "pipeline" processing and background subtraction for an equal comparison. For the IUE panel, the WFPC2 image has been convolved with a 6 arcsec FWHM function to simulate the IUE angular resolution within the large aperture (marked with white lines). Each frame is displayed in units of kR, with the same log intensity stretch.

W, but more typically a few $\times 10^{13}$ W. Of the three auroral regions, the majority of the luminosity and therefore input energy is in the main oval, although the polar regions can be comparable, particularly during a flare. These energy inputs occur at relatively fixed locations in Jupiter's atmosphere, so that standing dynamical patterns in the upper atmosphere are expected to be established in the redistribution to lower latitudes (see Chapter 9). By contrast, the satellite footprint emissions, of up to 10^{11} W (or locally tens of mW m^{-2}) for Io's footprint, represent energy input to constantly changing locations in the upper atmosphere. The footprint aurora is a transient feature spatially, in fact it would in places appear to cross from horizon to horizon in a period of minutes, if there were an observer there to see it. Auroral radio power (mostly non-Io-DAM) is difficult to estimate due to the poorly constrained longitude extent of the radio source. It is in the range 10^{10} to 10^{11} W, compared with $\sim 10^{12}$–10^{13} W in the IR and UV and $\sim 10^{9}$ W in X-rays. The *Galileo* Plasma Science (PLS) instrument has observed precipitation of electrons with energies of 0.1 to 10 keV between 6.8 R_J and 20–40 R_J, towards both hemispheres (Frank and Paterson 2002), corresponding to a precipitated power about 0.1–1 W m^{-2} in the auroral atmosphere. Such a large energy input in narrow auroral regions above the main oval can also strongly modify the ionosphere. A related phenomenon is the production of the auroral electrojet, which results from ion–neutral frictional drag produced by the breakdown in corotation in the middle magnetosphere (Huang and Hill 1989). This electrojet has been observed via Doppler motions in the H_3^+ emissions (Rego *et al.* 1999b, Miller *et al.* 2000).

Finally, a caution about relating auroral emissions to regions in Jupiter's magnetosphere. In a sense, the jovian upper atmosphere acts like a giant TV screen, responding to processes in the magnetosphere where particles are accelerated along field lines. In this analogy, the auroral morphology can be used to "map" from the auroral emissions out

along magnetic field lines to identify the regions in the magnetosphere where physical processes result in the accelerated particles. It is difficult in practice, however, to determine the mapping of an emission from a measurement of its latitude. At the distance of Io, a 1 R_J change in radial distance corresponds to a latitudinal shift of $\sim 2°$. While this level of accuracy can easily be achieved in HST images, the accuracy of the mapping decreases rapidly as one approaches the magnetic pole and the field strength increases. The uncertainty is magnified by the large azimuthal currents in Jupiter's middle magnetosphere, giving the local field a strong radial component which further "stretches" the radial distance between closely spaced field lines at the planet. For example, the magnetospheric plasma region between 20 R_J and 100 R_J maps into a latitudinal strip about 1° wide. The VIP4 model is not intended to be accurate beyond ~25–30 R_J, at these distances other models (Engle and Beard 1980, Khurana 1997) which include the effect of the current sheet may be used to estimate the local field.

26.1.10 The Earth's Aurora: Present Understanding

The story of our understanding of Jupiter's aurora begins at the Earth. With a long history of ground-based and spacecraft measurements, there exists a basic understanding of the physics of the Earth's auroral processes, which has formed the initial basis for interpretations of Jupiter's aurora. While a general picture of the nature of auroral activity on the Earth has evolved, there is still not a complete understanding of many details (Paschmann *et al.* 2002). It has been known for decades that auroral emissions are produced by high energy charged particles precipitating along magnetic field lines into the Earth's upper atmosphere from the magnetosphere (the region of space where the motions of particles are governed by the Earth's magnetic field). It is well established that the Earth's auroral activity is related to solar activity, and more specifically to conditions in the solar wind reaching the Earth. The precipitating charged particles are accelerated to high energies in the Earth's magnetosphere, with some acceleration occurring in the magnetotail region and some occurring by field-aligned potentials in the topside ionosphere. The auroral emissions then strongly modify the Earth's auroral ionosphere with large amounts of ionization and Joule heating. The Earth's auroral oval is known to maintain a pattern fixed with respect to the Earth–Sun line (i.e., along the noon–midnight meridian). The aurora normally exhibits oval shaped patterns centered on each magnetic pole, while the Earth rotates under these ovals. While the general orientation of the ovals may be fixed, large variations in auroral intensity (as well as the diameters of the auroral ovals) occur over time. The fixed ovals are due to the acceleration of particles in the interaction of the solar wind with the Earth's magnetic field. When auroral storms occur, they typically begin near local midnight with a brightening of one section of the auroral oval. The brightening will then extend along the oval, while at the same time the oval increases its radius, resulting in auroral displays that can be observed as far south as the southern USA.

Auroral storms on Earth occur when the interplanetary magnetic field (IMF) is southward, and large storms are generally produced when a coronal mass ejection on the Sun directs a high speed solarwind stream containing southward field towards the Earth. Such southward orientations result in the direct connection of the IMF and the Earth's magnetic field lines, via magnetic reconnection at the magnetopause boundary. The "open" field lines thereby produced are carried downstream from the Earth by the solar wind flow, and are stretched out into a long magnetic tail. Closed field lines return to the Earth via further reconnection in the tail. A large-scale magnetospheric flow is thereby set up by the solar wind interaction, modulated by the direction of the IMF. This flow is imposed on the collisional ionosphere via the magnetic field, setting up a large-scale system of currents flowing between the magnetosphere and ionosphere, which conveys stresses between them. The bright "discrete" auroral emissions at Earth correspond to regions of upward current flow out of the ionosphere, carried by hot magnetospheric electrons flowing down the field lines. This discussion smooths over many details, but should be sufficient to compare the processes which produce the aurora at Earth with those believed to be active at Jupiter.

26.1.11 Jupiter's Aurora: Post-*Voyager* Picture

The *Voyager 1* and *2* encounters and subsequent extended IUE observations led to a "standard" accepted picture of Jupiter's magnetosphere and the production of the polar UV auroras in the 1980s, which is outlined below. The *Pioneer* and *Voyager* missions provided the first in situ measurements of the strength and geometry of Jupiter's magnetic field and the plasma properties of the jovian magnetosphere. The *Voyager* missions also discovered Io's volcanoes, and revealed the full strength of the effects of the plasma torus on Jupiter's magnetosphere. The dominant mass source of plasma at Io leads to an immense current sheet which controls the dynamics of the middle magnetosphere. This is sometimes referred to as a "high β" magnetosphere (the β parameter is defined as the ratio of plasma pressure to magnetic field pressure) whose major source of plasma is internal. This contrasts with the Earth, where the solar wind interaction dominates auroral processes. The main solar wind effects at Jupiter are a noon–midnight asymmetry associated with the compression on the dayside, and the tail on the nightside. The solar wind pressure also leads to a dawn/dusk asymmetry to Jupiter's magnetosphere, and in this sense there are known to be diurnal variations in the magnetospheric dynamics. The exact dependence of magnetospheric processes and the aurora on solar wind and internal processes, however, are not yet well understood (see Chapter 24).

The resulting post-*Voyager* picture of Jupiter's magnetosphere was one filled with plasma predominantly from the Io torus, with the ions dominated by S and O species. It was believed that this plasma diffused slowly outward from the torus, and that some particles were accelerated to high energies by unknown processes. From estimates based on phase space density gradients, it appeared that these particles then diffused more rapidly back inwards, and were much less numerous inside ~10–15 jovian radii (R_J) (Gehrels and Stone 1983). The aurora were therefore thought to be produced by precipitating charged particles scattered in pitch angle into the loss cone at distances of 10–15 R_J. These would

have originated in the plasma torus, then been accelerated to high energies farther out in the magnetosphere. It was known that the corotating plasma in Jupiter's magnetosphere led to a current sheet which strongly distorted the local magnetic field outside ~6–8 R_J to many tens of R_J, with the region of corotating plasma out to ~20–25 R_J. Continuous currents from the magnetosphere to Jupiter's auroral ionosphere were believed to dissipate up to 10^{14} W of power in the very bright aurora. This auroral energy was known to be 20–50 times greater than the solar UV radiation absorbed globally in the upper atmosphere, so that the aurora would drive the upper atmosphere on a global basis. The ultimate source of energy for all these processes was Jupiter's rotation, which enforced pickup and corotation of the plasma via the magnetic field. This is in contrast to the situation at Earth, where the solar wind is the main source of energy for the aurora.

26.1.12 Correlations of Jupiter's Aurora with the Solar Wind

While Jupiter's main oval aurora is known to be energetically driven by the planet's rotation, the solar wind pressure still imparts an asymmetric shape to the magnetosphere. This asymmetry is known to be a strong factor in determining the dynamical patterns measured in Jupiter's outer magnetosphere (Vasyliunas 1983 and Chapter 24), and these exhibit characteristic local time behaviors. It may therefore be reasonably expected that the solar wind properties may influence Jupiter's aurora. Noting this, numerous authors have attempted to correlate measurements of auroral activity with the solar wind conditions at Jupiter. It should be noted that none of these studies to date has achieved the level of statistical certainty available for comparable studies at the Earth, and there are challenges to extrapolating the solar wind conditions from a distant point to Jupiter. The case of Jupiter is also different from that at the Earth due to the much longer travel times of solar wind disturbances past the much larger jovian magnetosphere. While a solar wind shock can move from the bow to the planet in a few minutes at the Earth, the same distance would be traveled in a few hours at Jupiter, and the disturbance would take several days to propagate down Jupiter's magnetotail. This should correspondingly impose a different dynamical response of Jupiter's magnetosphere to passing disturbances in the solar wind, compared with the Earth. With these caveats in mind, this section will briefly summarize reported correlations of the non-thermal radio emissions, then reported correlations of IR and UV auroral emissions.

Jupiter's strong magnetic field and rapid rotation result in a strong rotational control of magnetospheric phenomena and high repeatability of radio emission patterns (so-called "pulsar-like" behavior). The most precise determination of the core's rotation rate accordingly comes from long-term radio and magnetic field measurements (Higgins *et al.* 1997, Russell *et al.* 2001). Using *Galileo* PWS observations, intensifications of auroral radio components as well as of nKOM were discovered to be correlated with thickenings of the equatorial plasmasheet (Louarn *et al.* 1998), as well as with intensifications of UV auroral emissions (Prangé *et al.* 2001). These "energetic events" have been interpreted as being triggered by centrifugal ejections of plasma from Io's torus. The solar wind also exerts a notable influence, although secondary to rotation, on bKOM, HOM, and non-Io-DAM (Barrow *et al.* 1986, Barrow and Desch 1989) through its magnetic sector structure and density fluctuations, and a much weaker one, if any, on the Io-DAM (Zarka 1998). This may be attributed to the high latitude of the former radio sources, while the inner jovian magnetosphere and consequently the Io-DAM, produced in the Io flux tube (IFT) vicinity along $L \sim 6$ field lines, is more "insulated" from external conditions by closed jovian magnetic field lines. The detailed mechanisms of the solar wind influence remain unclear. They may involve reconnection processes in the magnetotail (Lepping *et al.* 1983) or at the magnetopause, modifications of the acceleration regions through parallel electric field buildup, or large-scale magnetospheric compressions (all processes which operate at the Earth). From the energetic point of view, whatever the mechanisms involved, the solar wind appears to contribute to driving the non-thermal radio emissions at all the magnetized planets, as supported by the scaling laws that have been derived between the overall radio power and the solar wind power input on the magnetospheric cross section (Desch and Kaiser 1984, Zarka *et al.* 2001b).

Evidence has been presented for statistical correlations of UV (Prangé *et al.* 1993) and H_3^+ (Baron *et al.* 1996) brightenings with solar wind pressure increases extrapolated to Jupiter from remote measurements over periods of months. Specific events in Jupiter's aurora have also been compared with extrapolated solar wind properties, indicating *no* correlation with a dawn storm observed in the UV (Ballester *et al.* 1996) but a positive correlation of the overall H_3^+ aurora (Connerney *et al.* 1996). Most recently, Gurnett *et al.* (2002) have reported increases in the HOM and UV emissions at times when interplanetary shocks were impinging on Jupiter's magnetosphere, as determined from *Cassini* and *Galileo* measurements close to Jupiter. These data have the advantage of good temporal sampling over a period of weeks and a minimal extrapolation of the solar wind conditions to Jupiter. Their measurements suggest a positive correlation between solar wind dynamic pressure and the overall intensity of the HOM and UV emissions based on two separate events, with the increase in UV auroral brightness being a factor of ~2 for the disc average brightness over a period of several hours. The Gurnett *et al.* (2002) measurements were not able to determine which of the auroral regions increased in brightness during that event. However, it also appears that the main oval brightened by a factor of ~2 on 13 January 2002 from STIS images, when the solar wind pressure at Jupiter was higher than average and the magnetosphere was compressed (Grodent *et al.* 2003a). The relation between these observations and theoretical expectations will be briefly discussed in Section 26.3.3 below. Grodent *et al.* (2003a) also report that the main oval contracted in latitude by up to 2° on that day, and that a similar contraction occurs systematically when each region of the main oval moves past local noon, where the effective solar wind pressure is at a maximum. Further theoretical work will be required to establish a clear physical interpretation of this contraction.

Taken in whole, the evidence favors a brightening of the total auroral emission during periods of increased solar wind dynamic pressure. It is to be emphasized, however, that a

range of processes are expected to take place in practice during the interaction between the jovian magnetosphere and complex time-dependent solar wind structures. In order to address these issues, and to resolve the various processes occurring, future study of more complete and well-determined data sets will be needed. Specifically, it will require extended intervals of spatially and temporally well-resolved observations of the jovian auroras, combined with reliable upstream solar wind measurements. Theoretical expectations for the main oval are discussed in Section 26.3.

26.2 THE IO INTERACTION AND SATELLITE MAGNETIC FOOTPRINT AURORA

The interaction of Io with Jupiter's magnetic field is of particular interest, with no equivalent phenomenon at the Earth. Io is electrically conducting by virtue of its ionosphere, with Jupiter's magnetic field and the corotating plasma torus sweeping past at a speed exceeding Io's orbital motion by 56 km s^{-1}. Following early DAM observations, a continuous electric current linking Io with Jupiter's ionosphere was proposed, driven by Io acting as a unipolar inductor with a 400 kilovolt potential induced across its diameter radially away from Jupiter (Piddington and Drake 1968, Goldreich and Lynden-Bell 1969). The *Voyager 1* spacecraft passed about 20 000 km south of Io, and found the local magnetic field and plasma flow distorted by a 3×10^6 ampere field-aligned current (Acuna *et al.* 1981) along Io's magnetic flux tube. The discovery of the plasma torus along Io's orbit implied that the field-aligned current would be carried by Alfvén waves propagating at a speed determined by the local plasma density (Belcher 1987). The measured torus plasma density suggested that the Alfvén waves carrying the current should return from Jupiter's ionosphere (Hill *et al.* 1983) after Io had passed beyond those magnetic field lines, so that the circuit would not maintain a direct current (DC) structure. Io's magnetic "footprint" auroral emission is produced at the point where the circuit is closed by currents in and out of Jupiter's upper atmosphere, detected for the first time by remote IR observations (Connerney *et al.* 1993). Jupiter's magnetic field also picks up ions and electrons from Io, distributing them into the corotating torus-shaped plasma region about Jupiter. Jupiter's rotation with an inclined and asymmetric magnetic field causes the torus to move north and south with respect to Io, thereby varying the current path length through the torus with longitude (in the opposite sense north and south). The field strength (and corresponding electric potential) at Io also varies by 20% with longitude. Considerable variability was therefore expected in the production of auroral emissions at Io's magnetic footprint on Jupiter, which would be diagnostic of the interaction of Io with Jupiter's magnetic field and the plasma torus.

As discussed below, different theoretical frameworks have been offered over the years to explain the Io interaction with Jupiter's magnetic field. The initial unipolar inductor mechanism explained well the early radio measurements, but the existence of the torus appeared to rule out a DC interaction between Io and Jupiter's ionosphere (Hill *et al.* 1983). The finding by *Galileo* of the magnitude and extent of the mass loading region near Io, and the corresponding slowing of field lines moving past Io, has once again changed the theoretical picture. In the following discussion, the measurements will be discussed in the context of what appears to be the most applicable theory. As more details have been learned, however, it has become clear that the nature of the interaction is complex, and requires detailed simulations for a good understanding (see Chapter 22).

26.2.1 Radio Emissions

The motion of Io through jovian magnetic field lines constitutes an electrodynamic generator. Whatever the exact mechanism driving this, it results in electron energization and precipitation of charged particles towards the planet. This leads to UV and IR auroral emissions at or near Io's magnetic flux tube footprint. The primary radio source corresponds to the bright auroral oval. At radio wavelengths, the Io-induced source only exists from the upper part of the HOM to the DAM range, i.e., from 1–2 MHz to 40 MHz, hence its name of "Io-DAM." It is attributed to the same microscopic generation mechanism as the auroral (non-Io) decameter emission (cf. review by Le Quéau 1988). Because its source has a limited longitudinal extent, being restricted to the vicinity of the Io flux tube (IFT), and because the radio beaming is very anisotropic, Io-DAM occurrence is limited to two specific ranges of Io's orbital phase, $\Phi_{Io} \sim 90°$ and $\sim 230°$ (so-called A and B sources of Io-DAM, Figure 26.4), corresponding to Io close to maximum east and west elongations from Jupiter. Io-induced radio emissions, as well as the associated UV and IR footprint emissions, are not produced along the instantaneous Io field line but along a flux tube threading Io's magnetospheric wake and thus "leading" Io by a few degrees relative to its orbital motion. The most recent estimates of this lead angle projected on to the surface of the planet are $\sim$0–10° in the south and up to $\sim$20° in the north from radio emissions (Queinnec and Zarka 1998), not inconsistent with IR and UV results of the auroral footprint locations.

At timescales of minutes to hours, jovian DAM is organized in "arcs" in the time–frequency plane (dynamic spectrum, see Figure 26.2). The specific shape of Io-DAM arcs has been attributed to the combination of strongly anisotropic emission beaming (in a conical sheet of 1–2° thickness opened at $\sim$70° from the local magnetic field) and of nonplanar field line shape (Queinnec and Zarka 1998, Kaiser *et al.* 2000). Radio fringes with $\sim$2 minute spacing observed to precede some Io-DAM arcs can be explained by multiple reflections of an Alfvén wave between Jupiter's ionosphere and the external boundary of the torus. Their counterpart in the UV and IR would be multiple spots separated by 1–2°. Multiple auroral emission peaks have occasionally been observed, but with a separation larger than 1–2° (Clarke *et al.* 2002a), together with a faint extended trail several tens of degrees long. At timescales <1 second, in very specific geometrical configurations Io–Jupiter–observer, Io-DAM arcs appear to consist of short-lived bursts (called S-bursts). They exhibit characteristics in common with the slowly varying Io-DAM emission (polarization, occurrence) but also many differences. They are generally more intense (up to 50 times), and are ten times less powerful on the average due to their instantaneous narrow band (a few kHz) (Queinnec and Zarka 2001). They have a fixed-frequency

duration of a few milliseconds, but drift very rapidly in the time–frequency plane, generally from high to low frequencies at -10 to -30 MHz s^{-1} (Ellis 1982). Observed average drift rates combined with present jovian magnetic field models imply that the emission is produced by electrons of $\sim$5 keV energy propagating adiabatically upwards from their mirror point (Zarka *et al.* 1996). However, the detailed burst microstructure is more complex (Carr and Reyes 1999). S-bursts could be attributed to the CMI mechanism, but their discrete nature is still unexplained.

Contrary to non-Io-DAM, HOM and bKOM, the Io-DAM activity is independent of solar wind fluctuations (Genova *et al.* 1987), probably because Io's flux tube is deeply embedded in the inner jovian magnetosphere. The fact that Io-DAM vanishes below 1–2 MHz, in spite of a minimum electron gyrofrequency reaching 60 kHz along the Io field line, has been attributed to the dense, extended cloud of plasma stagnating in Io's wake measured in situ by *Galileo* (Gurnett *et al.* 1996). It has been shown that protons in diffusive equilibrium along field lines threading through the wake may explain the CMI quenching below 1–2 MHz (Zarka *et al.* 2001a). Finally, extensive measurements by *Galileo*'s PWS experiment have revealed that Ganymede and perhaps Callisto also induce hecto-decameter radio emissions, through an electrodynamic interaction with the jovian field similar to Io's but much weaker (by about one order of magnitude in the case of Ganymede) (Hospodarsky *et al.* 2001). No effect has been found in the case of Europa. This is to be compared with the recent discoveries by HST of the UV footprints of all Galilean satellites but Callisto (Clarke *et al.* 2002a).

A scenario can be proposed linking radio emissions with UV and IR auroral emissions from the IFT footprint. Io-DAM is preferably emitted when Io is magnetically connected to negative surface field gradients in the direction of increasing longitude, corresponding to an increasing loss cone (Dessler and Hill 1979), and its occurrence was found to be anticorrelated with the brightness of the IR and UV auroral emissions near the IFT footprints (Genova and Calvert 1988, Connerney *et al.* 1993). This was interpreted as follows (Zarka *et al.* 1996). Alfvén waves produced at Io accelerate electrons which precipitate toward the planet. Some of these electrons are reflected due to the increase of magnetic field amplitude (adiabatic mirroring). Depending on this amplitude at the instantaneous IFT footprint, a variable fraction of precipitated electrons is lost through collisions and heating of the ionosphere, producing UV and IR emissions, while the rest is reflected back with a loss-cone distribution and is thus able to produce radio emission through the CMI. This explains the anticorrelation of optical and radio outputs, as well as the negative frequency drift of S-bursts (produced by upward propagating electrons). When the foot of the Io flux tube moves through negative surface field gradients (in the direction of increasing longitude), precipitating electrons "see" a decreasing surface field and are thus increasingly lost by collisions in the atmosphere. Such detrapping leads to an enhanced loss-cone distribution (both more empty and larger), more available free energy in the electron distribution, and thus an increased radio emission intensity (Galopeau *et al.* 2001).

Whatever the mechanism driving these processes, large amounts of energy are involved. Io-DAM power reaches 10^{9-10} W, while the IR and UV spots near the IFT footprints correspond to radiated powers of respectively 3–10×10^{10} W and 2–10×10^{10} W (Prangé *et al.* 1996, Satoh and Connerney 1999, Clarke *et al.* 2002a). These "optical" powers require a precipitated power $\sim 3 \times 10^{11}$ W in the form of 10–100 keV electrons, while in radio the CMI efficiency ($\sim$1%) implies a precipitating power of 10^{11-12} W in the 1–10 keV range. This is consistent with the $\sim 10^{12}$ W per hemisphere dissipated in the Io–Jupiter interaction (Neubauer 1980), and with an electron characteristic energy $\sim$5 keV as deduced from S-burst drift rates. In situ *Galileo* EPD and PLS measurements near Io have revealed bi-directional electron beams with energies in the range $\sim$0.1 to 100 keV and power of a few 10^{10} W (Williams *et al.* 1999, Frank and Paterson 1999). Such beams could provide enough power for the footprint electromagnetic emissions if they were to fill the Io flux tube. However, the question of the acceleration process is still open. The detection of bi-directional beams could result from upwards acceleration near the ionosphere by an Earth-like auroral potential structure, followed by mirroring. The remarkably large total precipitated power, $\sim 10^{11}$ W (equivalent to the Earth's total auroral power), concentrated in an area of a couple of hundred by $\sim$1000 km, must have strong consequences on the local atmosphere (see Chapter 9).

26.2.2 Conditions Near Io

Conditions at Io's end of the Jupiter–Io interaction may be expected to play an equally important role in the electrodynamic interaction between Jupiter and Io. *Galileo*'s Solid State Imager obtained high spatial resolution images of auroral emissions near Io (Geissler *et al.* 1999). The visible imagery captured several distinct emissions, the brightest of which was a blue glow, possibly due to molecular emission of SO_2, distributed about Io's equator, and brightest near the sub-Jupiter and anti-Jupiter limbs. There appears to be an association of this emission with known centers of volcanic activity on Io, as well as another association with the direction of the magnetic field at Io, which varies with Io's longitude. This component of the visible aurora appears to match the UV aurora studied extensively by Roesler *et al.* (1999) and Retherford *et al.* (2000), using HST STIS imagery of oxygen (135.6 nm) emissions. They demonstrated that this emission appears at the sub- and anti-Jupiter limbs, moving up and down in latitude so as to appear at the position of the tangent points of Jupiter's magnetic field. The intensity of UV emission increases the closer Io gets to the centrifugal equator, i.e., as increased plasma density is encountered as Jupiter rotates, and the anti-Jupiter spot appears brighter than the sub-Jupiter spot (Retherford *et al.* 2000).

Another component of the visible aurora, weaker than the equatorial glow and red in color, appears at each of Io's poles (Geissler *et al.* 1999). This emission, possibly due to atomic oxygen, is relatively bright at whichever pole is closest to the centrifugal equator. This emission is probably excited by electron impact on Io's atmosphere, but it is not clear how or even if this aurora is linked to that at the foot of the IFT in Jupiter's atmosphere. In the limit of a strong interaction, or closed loop model, in which the field lines are anchored in Io's ionosphere for a long time (many Alfvén travel times), one expects Io's polar aurora

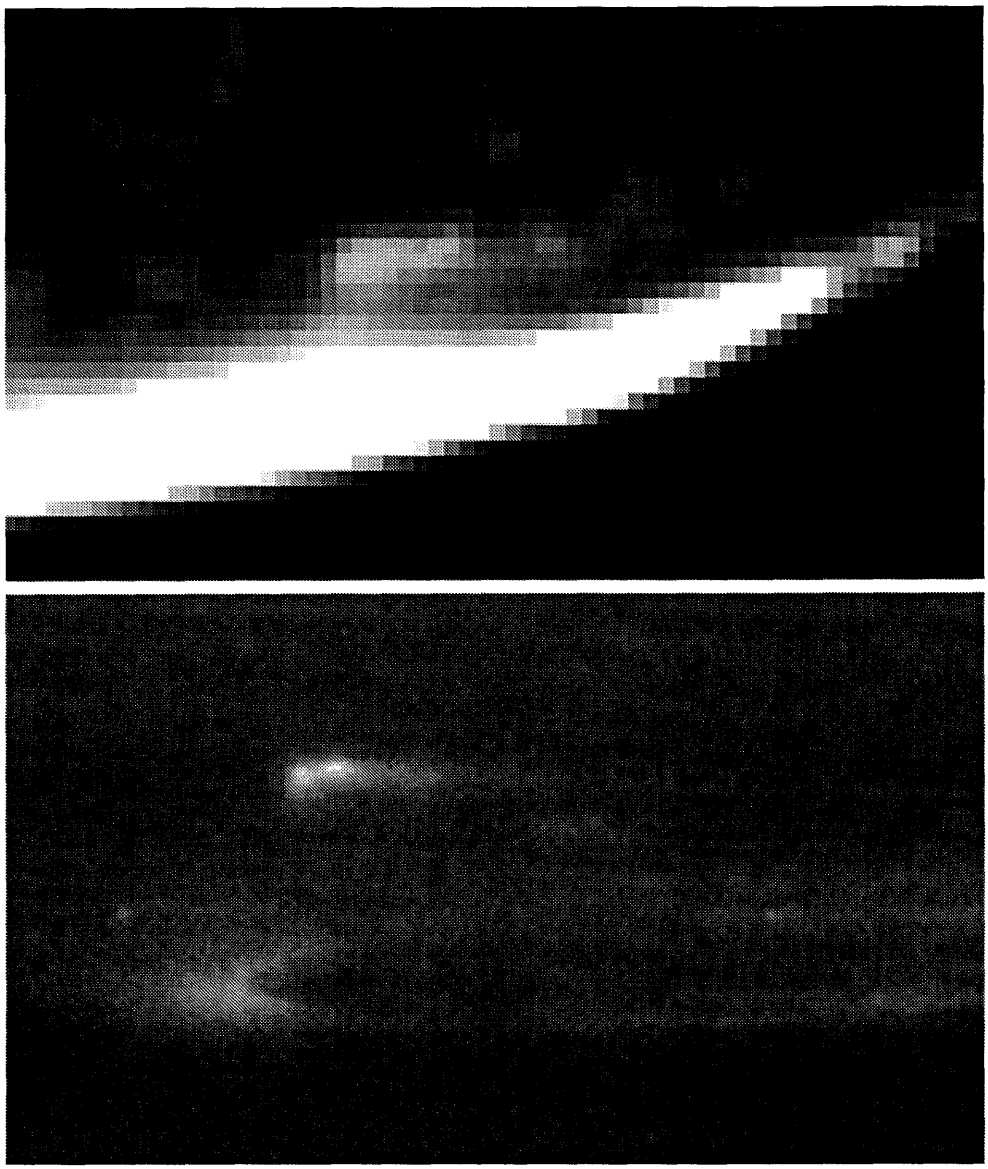

Figure 26.9. The auroral emissions from the Io footprint in the south exhibit structure, including a pattern of emissions extending in the downstream direction which at times includes a secondary maximum. (Upper) IR image of H_3^+ emissions from Jupiter's southern aurora taken with the NSFCAM on the IRTF telescope on 29 July 1998, with λ_{III}CML = 113° and Io phase = 193°. (Lower) HST STIS image of southern UV aurora on December 28, 2000, with λ_{III}CML = 62° and Io phase = 153°. Each frame covers 9 arcsec on a side, and no deconvolution or correction for limb brightening has been applied to either frame.

to brighten in concert with the aurora at the corresponding foot of the IFT in Jupiter's atmosphere. Observations of Io's aurora are as yet too sparse to separate dependencies on Io's longitude, local time, and intrinsic time variations. The equatorial emissions seen in both visible and UV images are likely due to the current system induced by the electromagnetic interaction (Retherford *et al.* 2000, Geissler *et al.* 1999) and there is good agreement between observation and simulated emissions (Saur *et al.* 1999, Chapter 22). It appears that the spatial distribution and intensity of Io's equatorial emissions are rather insensitive to the very large spatial variation in atmospheric density, and presumably ionospheric electron density, due to the distribution of volcanic plumes and frosty SO_2 patches (Hendrix *et al.* 1999). Measurement of ionospheric electron density at ten locations on Io's terminator by radio occultation (Hinson *et al.* 1998) confirms a substantial variation of peak electron density with location on Io, and is consistent with maximum electron densities near the sub- and anti-Jupiter points where UV emissions are brightest.

26.2.3 Io's Magnetic Footprint

The observed lead of the footprint auroral emission from Io's instantaneous magnetic flux tube also provides information on the nature of the interaction. In Goldreich and Lynden-Bell's unipolar inductor model, the lack of symmetry in the observation of radio waves from the Earth is explained by the twist imposed upon the IFT by a few $\times 10^6$ A of current flowing in the flux tube, closing in Jupiter's ionosphere.

The essential feature of this DC circuit model is the current closure in the ionosphere. The ionospheric footprint of the Io flux tube "leads" that of an undisturbed flux tube (one carrying no current) by about 10° for every 10^6 A of current carried by the flux tube and closing in the ionosphere. Changes in the circuit must be communicated by Alfvén waves traveling at the Alfvén velocity. The DC circuit model is applicable only if an Alfvén wave can propagate from Io to Jupiter and back again before the flux tube slips past Io. Post-*Voyager* theoretical models favored an "open loop" Io interaction, in which the two-way Alfvén wave travel time is too great to allow for current closure (Neubauer 1980, Bagenal 1983). In this case, Alfvén waves radiate away into space and may experience multiple reflections at density gradients in the torus or in Jupiter's ionosphere. The angle of propagation of the Alfvén wave (with respect to the magnetic field) depends on the density of the medium through which it propagates. Without current closure, the maximum "lead" of the foot of the flux tube is at most a few degrees, depending on how much high density torus plasma the wave propagates through before arriving at Jupiter. The Alfvén wave model allows for many reflections within the torus and between the torus and Jupiter's ionosphere (Neubauer 1980), creating a standing wave pattern that originates at Io and extends around the planet.

The first direct measurements of the position of Io's magnetic flux tube (IFT) footprint, compared with the O6 magnetic field model, were consistent with a "lead" of between 15° and 20° in accord with Goldreich and Lynden-Bell's DC circuit model (Connerney *et al.* 1993). The internal magnetic field model must be very accurate for this comparison, however, since one must compare the observed footprint position with a model "undisturbed" footprint. The position of a satellite footprint depends strongly on the actual field geometry near the surface of the planet. This is poorly constrained by the relatively distant spacecraft magnetic field measurements that have been available thus far. As a consequence, until recently the estimated uncertainty in the modeled Io flux tube footprint was comparable in magnitude to the expected lead angle (Connerney 1992). The accuracy of jovian magnetic field models improved greatly when the observed latitudes of the Io flux tube footprints were used as a constraint on the magnetic field geometry, leading to the VIP4 model (Connerney *et al.* 1998). Continued improvements in the magnetic field model are in progress. In the framework of the Alfvén wave model, the following conclusions regarding the lead of the IFT footprint can be summarized. In the northern hemisphere, the lead of the IFT footprint is a function of System III longitude, with a minimum lead angle of approximately 0° for 90°< sub-Io longitude <240° and a lead of 20° near zero longitude. In the south, there is no apparent dependence on System III longitude, and the lead angle in most observations falls in the range of 0–5°. The System III dependence of the lead angle in the northern hemisphere may be related to the expected variation of ionospheric Pedersen conductivity with surface magnetic field strength, as anticipated by the closed loop models of the interaction (Dessler and Hill 1979, Dessler and Chamberlain 1979). However, there is as yet no evidence for the local time variation in lead angle predicted by Goldreich and Lynden-Bell (1969) based on an ionospheric conductivity dominated by solar UV. This would be explained if along Io's L-shell charged particle precipitation greatly exceeds photoionization from solar UV radiation.

Recent observations have shown occasional multiple emission features along the locus of magnetic footprints of Io. Most commonly this appears as a distinct "double footprint" (Figure 26.9), documented in both H_3^+ IR images (Connerney and Satoh 2000) and in UV images (Clarke *et al.* 2002a), in which the IFT footprint appears as two emission peaks separated by ~4–12° of longitude along Io's orbital path. Peak emission intensities decrease in the downstream direction, and a continuous and gradually decreasing emission appears downstream of the instantaneous IFT foot, again observed in H_3^+, UV, and visible imagery. In contrast to the expected multiply reflected Alfvén waves propagating downstream of Io, the trailing emission has been attributed to the transfer of angular momentum to mass shed by Io as it is brought up to corotation by Jupiter's magnetic field (the "mass loading" process: Hill and Vasyliunas 2002, Delamere *et al.* 2003). *Galileo* measurements of the plasma properties near Io indicate that the interaction within 1–2 R_{Io} is largely driven by such mass loading, in contrast with a unipolar inductor process in the absence of a large plasma density. Spatially resolved spectra of the aurora obtained with STIS (Gérard *et al.* 2002) show that the mean energy of the electrons creating the northern UV emission ranges from about 55 keV at the Io footprint to ~40 keV at 20° downstream in the tail. In addition, the incident electron energy flux drops by a factor of ~6 over the same angular distance. These observations are consistent with the steady-state slippage picture, where the subcorotating flux tube is accelerated very slowly up to corotation due to nonideal coupling. In terms of the secondary peak, the measured low flow speed of flux tubes in Io's wake (Frank *et al.* 1996) implies that they will carry an initial Alfvénic current and lag behind corotation for ~1200 s after first contacting Io (Crary and Bagenal 1997). In the downstream region, the flux tubes are brought back up to corotation. The first and last field lines in this 1200 s interaction with Io correspond to an interval of 12° of Jupiter's rotation, and the observed secondary maxima extend a comparable distance downstream. One may therefore identify the brightest emissions from Io's footprint, including the secondary maximum, as driven by this interaction region near Io (Clarke *et al.* 2002a, Su *et al.* 2003).

No present theory of the Io interaction has sufficient detail to fully explain the IFT footprint observations. Some of the observations can be interpreted on the basis of the original unipolar inductor model, while others appear to require elements of the multiply-reflected Alfvén wave models, or hybrid versions of the Io interaction with the region near Io driven by mass loading. The effects of Jupiter's ionosphere on the circuit must also be taken into account (Shaposhnikov *et al.* 2001). These models may be considered the extreme solutions to a more general model that encompasses all these processes (see Chapter 22).

26.2.4 Other Satellites

UV auroral emissions have now also been detected from the magnetic footprints of Europa and Ganymede on Jupiter (Figure 26.1, Clarke *et al.* 2002a). Since Callisto's magnetic footprint overlaps the main oval auroral emissions, it is not

possible to detect comparably bright emissions, and little can be said about Callisto's interaction based on auroral images. One can estimate the induction potential across the other Galilean satellites, as has been done for Io. From the known diameters and orbital distances, plus in situ plasma motions from *Galileo* flyby measurements, one obtains potentials of 100 kV across Ganymede and 150 kV across Europa. There is evidence for the modulation of Jupiter's non-thermal radio emissions by Ganymede (Kurth *et al.* 2000), and the presence of an intrinsic magnetic field and external magnetosphere on Ganymede (Kivelson *et al.* 1996) presents the interesting possibility of a different electrodynamic interaction between this satellite and Jupiter. Taking the interaction region to be Ganymede's magnetosphere would increase the cross-sectional area and potential by a factor of four, comparable to the 400 kV potential across Io. Ganymede's interaction clearly leads to footprint emissions which are considerably brighter than Europa's. Localized UV emissions from Europa and Ganymede themselves have also been detected, indicating that auroral processes are active at these satellites (Hall *et al.* 1998, Feldman *et al.* 2000) at lower intensities than Io's airglow and auroral emissions. Io's footprint emissions at times reach several hundred kR in the UV, corresponding to inputs of tens of mW m^{-2}. This represents a large local power input to Jupiter's upper atmosphere and ionosphere, which is also transient. The auroral spots move rapidly east/west through Jupiter's upper atmosphere, as a result of the changing mapping due to each satellite's rapid motion through Jupiter's magnetic field. The emissions from the Ganymede and Europa footprints are generally a few tens of kRayleighs in brightness, corresponding to 1–5 mW m^{-2} or a total power of $1–5 \times 10^8$ W. This compares with up to 10^{11} W for the brightest Io footprint emissions, and about half that for the total downstream emissions.

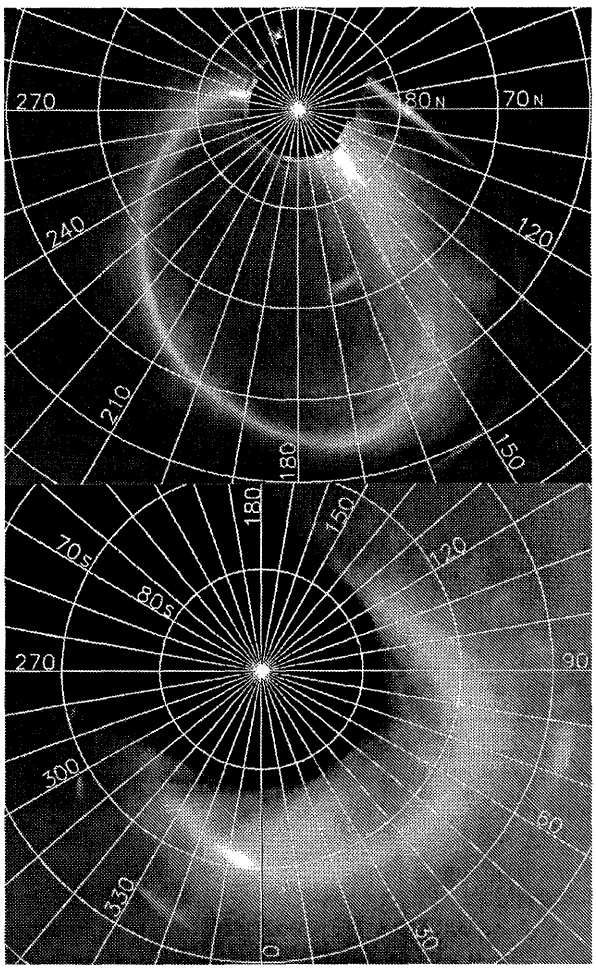

Figure 26.10. See Plate 14. Mean of all HST STIS images from December 2000–January 2001 projected to views from above the north (upper) and south (lower) polar regions. Data are from Grodent *et al.* (2003a). Grid lines indicate System III longitude and planetocentric latitude lines. The arcs of emission at the lowest latitudes are from the Io footprint on different days.

26.3 JUPITER'S MAIN AURORAL OVAL

The main oval auroral emissions, outlined in the introduction and illustrated in Figures 26.1 and 26.10, are essentially continuously present and located in circumpolar bands around both northern and southern magnetic poles at ~15° magnetic co-latitude (defined here simply as the spherical polar co-latitude measured from the magnetic dipole axis). The observed discrete emission features corotate with the planet at the System III rotation period, thus indicating magnetic field control (Ballester *et al.* 1996, Grodent *et al.* 2003a). The ovals are very narrow and very bright. The overall width is ~100–500 km, in which region the brightness exceeds ~100 kR at visible and UV wavelengths, peaking at up to MR intensities (Ballester *et al.* 1996, Prangé *et al.* 1998, Vasavada *et al.* 1999). The average distributions of the UV auroral emissions about each pole are displayed in Figure 26.10. The locations of the H_3^+ and visible (nightside) emissions are similar to the UV distribution, with some significant differences discussed below.

During the *Cassini* flyby HST observing campaign in December 2000–January 2001 the brightness was found to vary by only a few tens of percent about the mean on a daily-averaged basis, with extrema of less than a factor of two about the mean for individual intervals (Grodent *et al.* 2003a). However, dynamical features are also present, the most pronounced of which are the "dawn storms". These appear as faint structured emissions near the poleward border of the main oval in the dawn local time sector, which then intensify to a brightness of several MR on a timescale of approximately 1 hour (Gérard *et al.* 1994b, Ballester *et al.* 1996, Clarke *et al.* 1998). Once formed, the "storm" arcs appear to remain fixed in local time near magnetic local dawn, giving rise to the appellation "dawn storms". Similar emissions have also been observed in Saturn's aurora (Trauger *et al.* 1998), implying common processes in the giant planet magnetospheres. Observed in more detail with STIS, a storm-like event in a similar location showed auroral arcs originating clearly poleward of the main oval and locked in corotation (Grodent *et al.* 2003a). These emissions moved down on to the main oval as they brightened, and appear to have evolved into a dawn storm. This would imply that this storm was triggered somewhere in the outer magnetosphere, and may have initiated a disturbance which propagated into the main oval source region.

Within this framework, Hill (1979, 2001) suggested that the main jovian auroral oval is connected with the magnetosphere–ionosphere coupling current system associated with the breakdown of rigid corotation in the middle magnetosphere region. The main auroral oval may thus result from the upward Birkeland current that enforces partial corotation of plasma moving outward from the Io plasma torus. Estimation of the field-aligned currents (Cowley and Bunce 2001) suggest the existence of field-aligned voltages of order ~100 kV responsible for the acceleration of primary auroral electrons up to ~100 keV, producing an auroral brightness of a few megaRayleighs in agreement with the images. This mechanism may also be connected indirectly (e.g., by plasma heating under the acceleration region) with the detection of intense field-aligned beams near the equator between 20–30 R_J (Frank and Paterson 2002).

Indications of the physical origins of these emissions can be obtained both from the nature of the precipitating particles and from their location. With regard to the primary incident particles, while some uncertainties remain, observations of the emission altitude and UV emission spectra indicate that electrons spanning the energy range up to many tens of keV must be the dominant component (Ajello *et al.* 1998). Energetic sulfur and oxygen ions would give rise to UV emission lines of S and O which have not been observed (Waite *et al.* 1988), and Doppler-shifted H Lyα emission characteristic of fast precipitating protons has also not been observed (Clarke *et al.* 1989, Rego *et al.* 1999a), placing strict limits on the possible contributions of primary particles other than electrons. With regard to location, the mapping to distances greater than ~20 R_J is now well established from the fact that the main oval is displaced distinctly poleward of the auroral emissions associated with the magnetic footprints of the moons: Io (~6 R_J), Europa (~9 R_J), and Ganymede (~15 R_J) (Clarke *et al.* 2002a). The mapping to less than ~30 R_J is based on the observation that discrete features in the main oval are close to corotating, which implies mapping to a region where the plasma is correspondingly close to corotation.

26.3.1 Theoretical Ideas of the Origin of the Main Oval

Theoretical discussion of the main oval was initiated by Thorne (1983), who focused on wave-driven pitch-angle diffusion of hot magnetospheric plasma. Wave amplitudes were suggested to be large enough to maintain a full loss cone, and thus to result in precipitation at the maximum "strong diffusion" rate. However, the resulting precipitating energy fluxes were found to be only ~0.1–1 mW m^{-2}, sufficient at ~20% conversion efficiency to produce an aurora of 1–10 kR intensity, lower than those required by two to three orders of magnitude. Similar conclusions have been reported most recently by Tsurutani *et al.* (1997), who examined the hypothesis using *Ulysses* data that the main auroral oval is created by wave diffusion of magnetospheric plasma in the magnetopause boundary layer.

Jovian auroral emissions have also been discussed in relation to field-aligned current systems that may generate energetic electron precipitation in regions of upward current flow. The first such suggestion was made by Kennel and Coroniti (1975) in relation to the coupling of angular momentum between the ionosphere and magnetosphere in a solar wind-like radial outflow plasma model which was then under discussion. Isbell *et al.* (1984) also discussed the field-aligned currents and related aurora which would be excited by the interaction between the solar wind and a rapidly rotating magnetised planet, which twists up the open field lines in the tail lobes. However, the magnetic mapping discussed above implies a mapping deeper inside the magnetosphere, hence it seems pertinent to discuss field-aligned currents which map to the middle magnetosphere region at equatorial distances of several tens of R_J (Gérard *et al.* 1994a, Dougherty *et al.* 1993). Most recent discussion has thus related the main oval auroras to the middle magnetosphere system of currents which is associated with the maintenance of corotation in outwardly diffusing iogenic plasma (Hill 1979, Vasyliunas 1983, Barbosa 1984). The following discussion therefore expands on these models, focusing on new results presented by Bunce and Cowley (2001b), Cowley and Bunce (2001), Hill (2001), and Southwood and Kivelson (2001). It begins, however, with a brief review of the relevant physical background.

The most important factor governing the physics of the jovian middle magnetosphere is the massive source of plasma

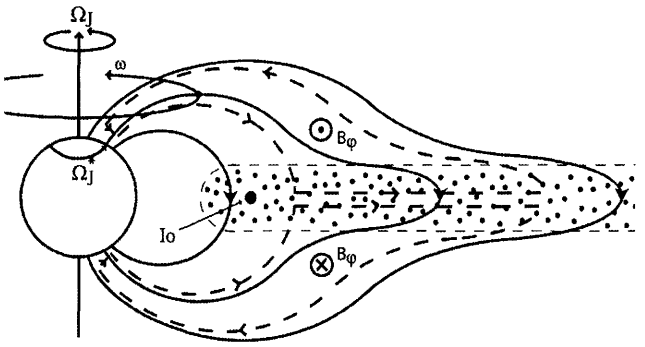

Figure 26.11. Sketch of a meridian cross section through the jovian magnetosphere, showing the principal features of the inner and middle magnetosphere regions. The arrowed solid lines indicate magnetic field lines, which are distended outwards in the middle magnetosphere region by azimuthal currents in the current sheet. The current sheet plasma originates mainly at Io, which orbits in the inner magnetosphere at ~6 R_J as indicated, liberating ~1000 kg s^{-1} of sulfur and oxygen plasma. This plasma is shown by the dotted region, which rotates rapidly with the planetary field due to magnetosphere–ionosphere coupling, while more slowly diffusing outwards. Three separate angular velocities associated with this coupling are indicated. These are the angular velocity of the planet Ω_J, the angular velocity of a particular shell of field lines ω, and the angular velocity of the neutral upper atmosphere in the Pedersen layer of the ionosphere, Ω_J^*. The latter is expected to lie between ω and Ω_J because of the frictional torque on the atmosphere due to ion–neutral collisions. The oppositely-directed frictional torque on the magnetospheric flux tubes is communicated to the equatorial plasma by the current system indicated by the arrowed dashed lines, shown here for the case of subcorotation of the plasma (i.e., $\omega \leq \Omega_J$). This current system bends the field lines out of meridian planes into a "lagging" configuration, associated with the azimuthal field components B_φ shown.

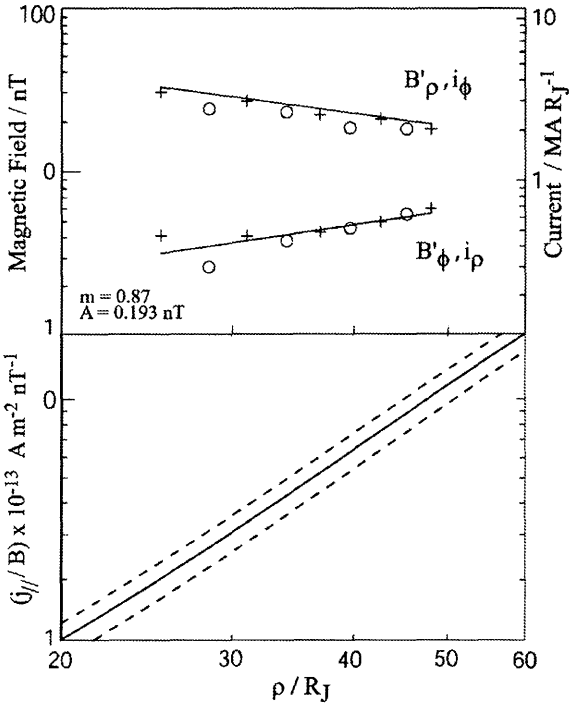

Figure 26.12. The top panel shows radial profiles of B'_φ and B'_ρ determined between ~25 and ~50 R_J on the outbound trajectory of *Voyager 2*, averaged over intervals when the spacecraft was located outside of the current sheet. The prime indicates that the internal planetary field has been subtracted from these data, and a small latitude correction has also been applied to the radial field data. The left-hand scale shows the magnetic field strength in nT, while the right-hand scale indicates the corresponding current intensity in the current sheet in MA R_J^{-1}, given by Equation (26.2). Field averages obtained north of the current sheet are shown as crosses, while those obtained south of the current sheet are shown as circles. Azimuthal averages obtained north of the sheet and radial averages obtained south of the sheet have had their signs reversed so that all values are positive. The lower panel shows the corresponding radial profile of $(j_{||}/B)$, obtained from Equation (26.4), and shown for the northern hemisphere, such that positive values indicate a flow of field-aligned current from the ionosphere to the current sheet (adapted from Bunce and Cowley 2001b).

at Io, which orbits deep within the equatorial magnetosphere at a radial distance of ~6 R_J. The iogenic plasma, consisting mainly of sulphur and oxygen ions (plus electrons), forms a dense torus in the vicinity of Io's orbit, which is confined to the equatorial region by the centrifugal action of the near-corotating flow (Bagenal 1994, Chapter 23). However, the torus is unstable to centrifugally-driven flux tube interchange motions, resulting in outward radial diffusion of the cool dense plasma to form an equatorial plasma disc. At the same time, hot tenuous plasma from the outer magnetosphere diffuses inward, thus forming a two-component hot–cool plasma. The outward-directed pressure gradient force, due primarily to the hot plasma, and the similarly outward-directed centrifugal force, due primarily to the cool plasma, then distend the middle magnetosphere field lines outward from the planet in the equatorial region, such that the outward-directed plasma forces are balanced by the inward-directed force of the field tension (Caudal 1986). The latter tension force is just the $j \times B$ force produced by the eastward azimuthal current flowing in the equatorial plasma associated with the outward field distension, combined with the north–south field threading through the equator. The resulting field and plasma structure is illustrated in Figure 26.11, which shows a cut through the system in a magnetic meridian plane. The arrowed solid lines are magnetic field lines, while the region occupied by the outwardly diffusing iogenic plasma is shown by the dotted region. The field lines which thread this plasma define the middle magnetosphere, which thus extends outward in the equatorial plane from the inner edge of the torus at ~5 R_J towards the magnetopause, even though the plasma currents are sufficient to distend the planetary field significantly only at equatorial distances beyond ~15 R_J. As we will see below, the radial distension of the field into a "current sheet" configuration in the more distant middle magnetosphere proves to be an important ingredient in determining the intensity of the main oval emissions.

As the iogenic plasma diffuses outward, its angular velocity (ω in Figure 26.11) falls due to conservation of angular momentum. If there is no torque acting on the plasma, ω will fall inversely as the square of the distance. However, when the angular velocity falls below that of the planet (Ω_J), or more specifically that of the neutral atmosphere at the feet of the field lines (Ω_J^*), ion–neutral collisions take place in the Pedersen layer of the ionosphere which produce a frictional torque on the plasma which spins it back up towards corotation with the planet. This torque is conveyed to the equatorial plasma via the magnetic field, which is bent out of meridian planes into a "lagging" configuration, associated with azimuthal perturbation fields (marked B_φ in Figure 26.11) which reverse in sense across the equatorial plane. The corresponding electric current system, of primary interest here, is shown by the dashed lines in Figure 26.11. Equatorward-directed Pedersen currents in the ionosphere are connected to outward radial currents flowing in the equatorial plane via a large-scale system of field-aligned currents flowing between them (Hill 1979, Vasyliunas 1983). The torque associated with the $j \times B$ force of the Pedersen currents balances the frictional torque of the atmosphere, while the equal and opposite torque associated with the $j \times B$ force of the equatorial current (the field tension force of the "lagging" field) accelerates the iogenic plasma in the sense of corotation. The field-aligned currents which connect the two field-perpendicular currents flow away from the planet in the inner part of the system, while reversing to flow toward the planet in the outer part. It is thus suggested that the electron precipitation associated with the main oval auroras is related to the former of these regions of field-aligned current. Confirmation of this current system was provided by the direct measurement of the H_3^+ ion flow along the main oval (Rego *et al.* 1999, Stallard 2001). The poleward closure currents and their relation to the polar aurora will be discussed further in Section 26.4.3.

26.3.2 Estimates of Field-aligned Current Densities from Spacecraft Magnetometer Data

The strength of the field-aligned currents in the middle magnetosphere can be estimated by analysis of spacecraft magnetometer data, as recently shown by Bunce and Cow-

ley (2001b) and Khurana (2001). This is illustrated in Figure 26.12, where the essentially radial profiles of the cylindrical radial and azimuthal currents on the outbound pass of *Voyager 2* (at a magnetic local time of ~01:30 MLT) determined in the former of these studies are shown. These have been determined by averaging the azimuthal and radial field components, respectively, during intervals in which the spacecraft was located outside of the current sheet. Assuming that the sheet can be treated as a semi-infinite thin slab with equal and opposite fields on either side, the integrated current intensity in the layer (A m^{-1}) can be approximated as

$$i \approx \pm \frac{2}{\mu_o} [-B_\varphi \hat{\rho} + B_\rho \hat{\varphi}] \tag{26.1}$$

where the upper sign corresponds to observations north of the sheet, and the lower sign to observations south of the sheet. It can be seen that over the radial range considered (~25–50 R_J), the radial current intensity increased with distance, while the azimuthal current intensity fell.

The field-aligned current emerging from the upper and lower faces of the current sheet and connecting to the ionosphere, assumed equal and opposite in the northern and southern hemisphere, is then given by the divergence of the sheet current

$$\frac{j_{||}}{B} = \frac{j_z}{B_z} = -\frac{1}{2\rho B_z} \left[\frac{\partial (\rho i_\rho)}{\partial \rho} + \frac{\partial i_\varphi}{\partial \varphi} \right] \tag{26.2}$$

The quantity $\left(j_{||}/B\right)$ has been formed because it is conserved along the field lines between the equator and the ionosphere in the region where the field-perpendicular currents are taken to be negligible. The first term in the bracket can be determined directly from the radial profile of i_ρ shown in the upper panel of Figure 26.12, while the second term in the bracket represents (in this case) a small correction associated with the local time dependence of the azimuthal current. This has been estimated by Bunce and Cowley (2001a) from the local time dependence of the radial field on several flyby trajectories times, and updated by Bunce *et al.* (2002) to include data from *Galileo* (which has been employed here in Figure 26.12). The north–south field B_z which threads the current sheet is also required, given by the *Voyager 2* empirical model derived by Khurana and Kivelson (1993). The radial profile of $\left(j_{||}/B\right)$ along the *Voyager 2* trajectory so determined is shown in the lower panel of Figure 26.12. It can be seen that the values are positive, implying a current flow from the ionosphere into the current sheet, and increase with distance, from 10^{-13}A $m^{-2}nT^{-1}$ at ~20 R_J, to 10^{-12}A $m^{-2}nT^{-1}$ at ~50 R_J. Since $\left(j_{||}/B\right)$ is conserved along the field lines, it is then possible to estimate the field-aligned current density at ionospheric heights by multiplication by the strength of the polar ionospheric magnetic field (~850 000 nT), yielding values ~0.1–1 mA m^{-2}. These are appreciably large values, not dissimilar from those characteristic of the large-scale field-aligned current systems at Earth.

Bunce and Cowley (2001b) also considered the conditions under which such currents can flow above the jovian ionosphere. Estimates based on Knight's (1973) kinetic theory and *Voyager* estimates of magnetospheric electron parameters outside the current sheet suggest that substantial field-aligned voltages are required, of order ~100 kV. Saur

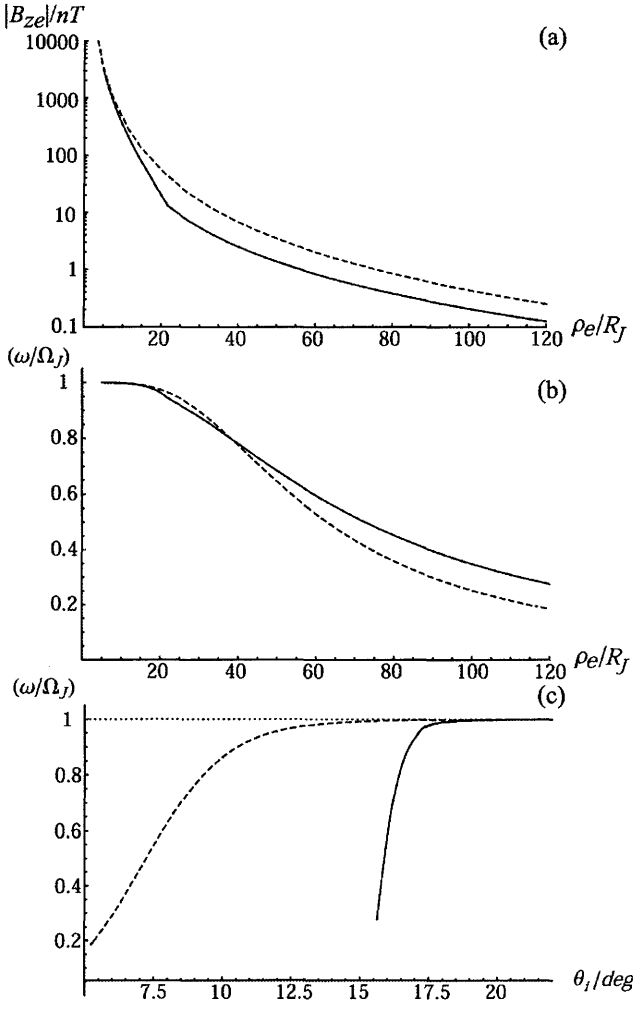

Figure 26.13. (a) Log–linear plot of the modulus of the north–south field component B_{ze} (nT) which threads the current sheet versus equatorial radial distance ρ_e (R_J), showing (dashed) the planetary dipole field and (solid) the empirically-based current sheet model as described in the text. The actual values of B_{ze} are all negative. (b) Self-consistent steady-state equatorial plasma angular velocity profile (normalised to the planetary angular velocity Ω_J) for the dipole field (dashed) and current sheet model (solid), obtained from integration of Equation (26.4) with $\Sigma_P^* =$ 0.5 mho and $\dot{M} = 1000$ kg s^{-1}. Rigid corotation has been imposed as a boundary condition at 5 R_J. (c) The angular velocity profiles shown projected along the model field lines into the ionosphere, plotted versus dipole co-latitude. The dotted line shows the condition for rigid corotation.

et al. (2003) have also suggested that such voltages could be generated by the weak turbulence observed by *Galileo* in the middle magnetosphere. When such voltages are included, the precipitating energy flux of magnetospheric electrons increases by orders of magnitude, from a maximum value of ~0.1 mW m^{-2} without acceleration (corresponding to the strong diffusion limit mentioned above) to ~10–100 mW m^{-2}, sufficient to produce ~0.1–1 MR auroras. Bunce and Cowley (2001b) thus suggested a direct connection between the current system inferred from the spacecraft data and the main oval emissions.

26.3.3 Theoretical Models

Motivated by these results, Cowley and Bunce (2001) set up a theoretical model which allows explicit calculation of the middle magnetosphere current system and related auroral parameters. The essential ingredients are empirical (observation-based) models of both the equatorial magnetic field and the equatorial angular velocity profile of the plasma. The plasma flow is mapped along the field lines to the ionosphere using the magnetic model, the ionospheric Pedersen current i_P calculated from the electric field in the neutral atmosphere rest frame and the Pedersen conductivity Σ_P, and the radial current in the equatorial plane i_ρ from

$$\rho_c i_\rho = 2\rho_i i_P \tag{26.3}$$

since it is evident from Figure 26.11 that the equatorial current crossing a given flux shell in a given azimuth sector must be equal to the sum of the two ionospheric currents crossing the same shell in the same sector. In Eq. (26.3) ρ_c is the equatorial radial distance of the flux shell, while ρ_i is the ionospheric distance of the flux shell from the magnetic axis. The field-aligned current can then be calculated from the divergence of either the ionospheric or equatorial field-perpendicular current. The calculation is completed by employing Knight's (1973) theory to estimate the field-aligned voltages required to generate the field-aligned current, and the resulting precipitating electron energy flux. Cowley and Bunce's (2001) model was found to generate upward-directed field-aligned currents throughout the middle magnetosphere region, which map to the ionosphere in circumpolar rings of latitudinal width $\sim 1°$ ($\sim$1000 km), centered near $\sim 16°$ dipole co-latitude. Peak current densities were found to be $\sim$ 1 mA m^{-2} in conformity with the above results, requiring field-aligned voltages of $\sim$100 kV for typical magnetospheric electron parameters, and which result in precipitated energy fluxes of $\sim$100 mW m^{-2} sufficient to drive $\sim$1 MR UV auroras.

In a parallel study, Hill (2001) determined the field-aligned currents associated with his original model of corotation breakdown (Hill 1979). The calculation is conceptually similar to that above, but differs in a number of respects. Most importantly, the magnetic field is taken to be a dipole field rather than an empirically-based current sheet, while the angular velocity profile is calculated self-consistently (as in the original study) rather than being an empirical "guess". Hill (2001) found that the upward current in this model maps to a ring in the ionosphere $\sim 5°$ wide, centered near $\sim 10°$ dipole co-latitude. The peak upward current density at ionospheric heights was found to be $\sim$0.03 mA m^{-2}, more than an order of magnitude less than the above estimates.

The reasons for these large quantitative differences have been examined by Cowley *et al.* (2002, 2003a), and results from these calculations will be presented here since they encapsulate the results of both studies. Figure 26.13 shows a log–linear plot of the modulus of the north–south field B_{ze} versus ρ_e. The dashed line shows the dipole field employed by Hill (2001), while the solid line shows the empirical current sheet model employed by Cowley and Bunce (2001). The latter consists of two segments, determined from the Connerney *et al.* (1981) model for small ρ_e, and the Khurana and Kivelson (1993) model at large ρ_e. The empirical

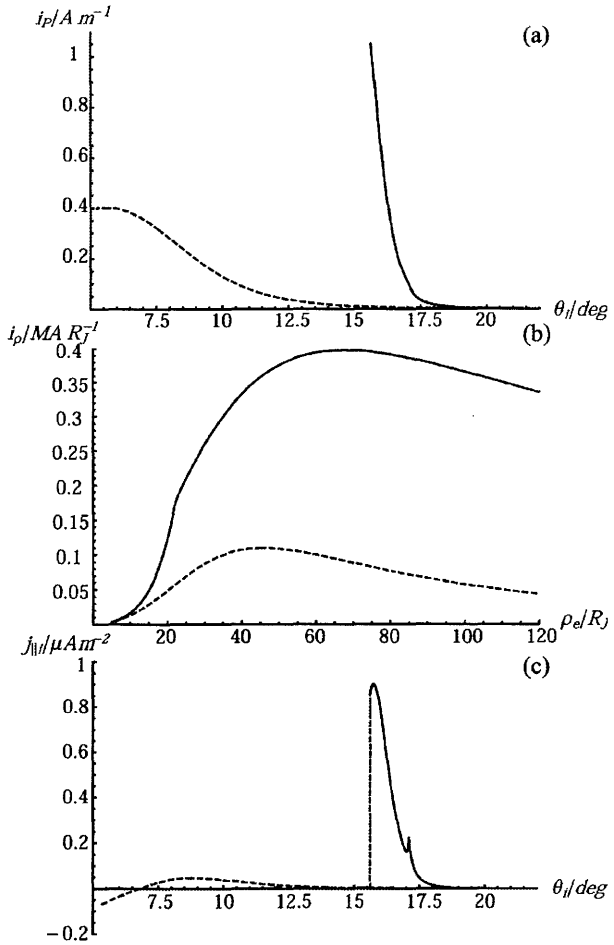

Figure 26.14. (a) Plot of the height-integrated Pedersen current in the ionosphere versus dipole co-latitude for both dipole (dashed) and current sheet field (solid) magnetic models, determined from the angular velocity profiles shown in Figure 26.13c. (b) Plot of the corresponding equatorial current intensities, obtained from Eq. (26.3), shown versus equatorial radial distance. (c) Plot of the corresponding field-aligned current distributions, shown as the ionospheric field-aligned current density (where we have taken $B_i = 2B_J$) versus dipole co-latitude. The vertical short-dashed line which terminates the current sheet model profile (solid line) marks the outer boundary of the current sheet region considered here, at an equatorial radial distance of 120 R_J.

values are significantly less than those of the dipole beyond $\sim$15 R_J, reflecting the stretched-out nature of the current sheet field lines.

The self-consistent angular velocity profiles of the equatorial plasma are then calculated for each model using Newton's second law (Hill 1979, Pontius 1997), i.e.,

$$\frac{\mathrm{d}}{\mathrm{d}\rho_e}\left(\rho_e^2\omega\left(\rho_e\right)\right) = \frac{2\pi\rho_c^2 i_\rho \left|B_{ze}\right|}{\dot{M}} \tag{26.4}$$

where the left side is the radial gradient of the plasma angular momentum per unit mass, while the right side is the electromagnetic torque per unit radius per unit mass acting on the equatorial plasma. $\dot{M}$ is the mass outflow rate from the Io torus, taken to be 1000 kg s^{-1}. Solutions obtained assuming rigid corotation at 5 R_J (the inner edge of the torus)

are shown in Figure 26.13b, where again the dashed line is for the dipole model, and the solid line for the current sheet model. The effective ionospheric Pedersen conductivity Σ_P (reduced from the true value due to possible slippage of the neutral atmosphere in the Pedersen layer due to ion–neutral collisions) has been taken to be 0.5 mho. The angular velocity profiles for the two fields are similar, in agreement with the results of Pontius (1997). Physically, this results from the fact that while the equatorial B_{ze} field is weaker for the current sheet model than for the dipole, the radial current is stronger (as will be seen below), such that the two effects approximately cancel to give similar radial profiles of the azimuthal $j \times B$ force which acts to maintain corotation. However, a substantial difference occurs when the angular velocities are mapped to the ionosphere, as shown in Figure 26.13c. Here (ω/Ω_J) is plotted versus dipole co-latitude θ_i. The departure from rigid corotation takes place much closer to the pole for the dipole than for the current sheet model, and over a considerably larger range of co-latitudes.

Figure 26.14a shows the corresponding ionospheric Pedersen current, where it can be seen that the currents for the dipole field are less than those for the current sheet model by factors of 2–3. This results from the fact that field lines of a given angular velocity map closer to the pole for the dipole than for the current sheet, such that the velocity of the plasma in the planet's rest frame is less for the former than for the latter, so the electric fields and currents are also less. Consequently, as shown in Eq. (26.3) and Figure 26.14b, the equatorial current is also less. The equatorial currents can be compared directly with the observed currents shown in Figure 26.12. The current sheet model profile increases over the relevant radial range in a similar manner to those observed, and the magnitudes are also similar, if a little lower (no attempt at "fitting" has been made). By comparison, the dipole values are lower than those observed by almost an order of magnitude.

The field-aligned current density at ionospheric heights is shown in Figure 26.14c. The profile for the current sheet model is consistently positive (outward current) and sharply-peaked over ~1° at ~16° co-latitude, with a peak value of 0.9 μA m^{-2}, similar to the results found by Cowley and Bunce (2001). (Note that the secondary maximum near 17° occurs at the transition from one magnetic field description to the other in the current sheet model and is artificial.) Results for the dipole field, on the other hand, show a broad positive profile ~6° wide with a maximum value of 0.05 μA m^{-2} at 8.9°, followed by a reversal to negative (inward) currents poleward of 6.8°, similar to the previous results of Hill (2001). The background magnetic field and its mapping to the ionosphere is therefore of crucial significance in determining the field-aligned current flow.

The same is also true of the auroral parameters. In Figure 26.15 the resulting field-aligned accelerating voltage and precipitating energy flux are shown, respectively, computed using Knight's (1973) kinetic theory using a magnetospheric electron density and temperature of 0.01 cm^{-3} and 2.5 keV, respectively, based on *Voyager* data (Scudder *et al.* 1981). For the current sheet model the accelerating voltage peaks at ~16° with a maximum value of 165 kV, and falls off sharply on either side. The resulting variation with latitude in the mean precipitating electron energy is in principle testable using high resolution color-ratio maps. For the dipole model

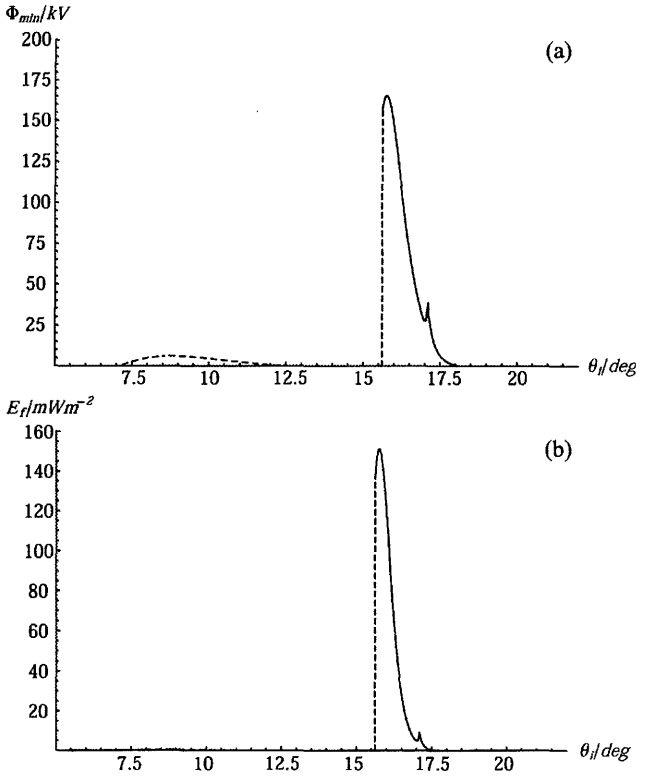

Figure 26.15. (a) Field-aligned voltage profiles are shown for both the dipole field model (dashed line) and for the current sheet model (solid line), plotted versus dipole co-latitude, determined from Knight's (1973) theory applied to regions of upward field-aligned current. (b) The precipitating electron energy flux is plotted versus dipole co-latitude for both the dipole field model and the current sheet model. The dipole values are almost too small to register (peaking near ~9°) on this plot.

the profile is spread in latitude about a peak at ~9°, and with a much reduced maximum value of 6 kV. The energy flux for the current sheet model peaks at 150 mW m^{-2}, sufficient to produce a UV aurora in excess of ~1 MR intensity, comparable to main oval intensities. The flux falls to half this value across a narrow strip whose full latitude width is 0.6° (~700 km). The energy flux associated with the dipole model is almost too small to register on this plot, and peaks at a value of ~0.4 mW m^{-2}, with the overall distribution being capable of producing a few-kR aurora over a latitude region ~3° wide. The very different latitude positions, widths, and intensities of the auroral distributions in the two cases again emphasizes the crucial role played by the background magnetic structure and the ionospheric mapping. We also note that in the current sheet case the auroral primaries are electrons of ~100 keV energy, such that the auroral acceleration region is a substantial source of relatively high-energy particles. However, it seems likely that wave–particle interactions beneath the voltage drop (located typically 2–3 R_J above the ionosphere) will significantly scatter the primary beam before it reaches the ionosphere, such that the electrons which precipitate and excite the aurora will be substantially spread in energy.

Given these ideas for the basic mechanism of the main oval auroras, it is possible to briefly discuss their expected dependence on interplanetary conditions. The role of the

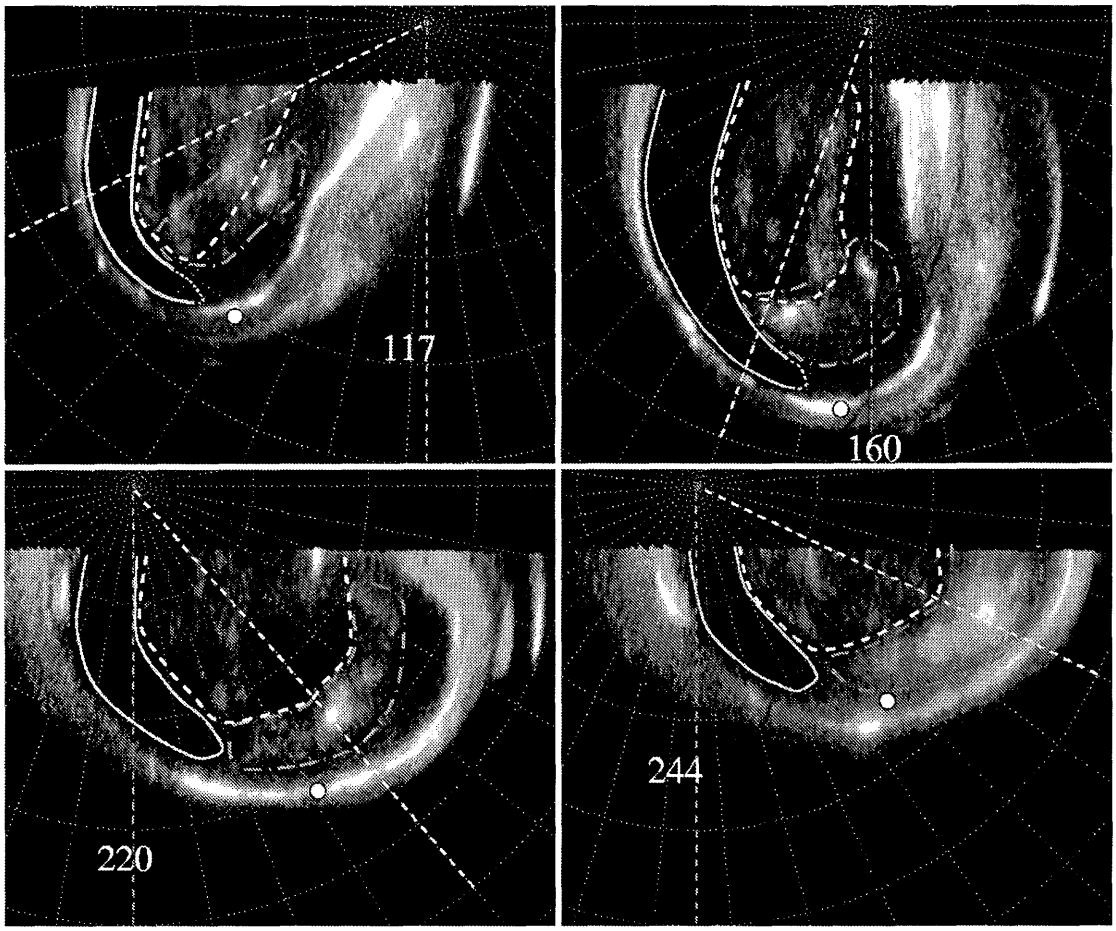

Figure 26.16. Polar projections of Jupiter's aurora from STIS UV images on December 16, 2000 (Grodent *et al.* 2003b). Polar emission regions outlined are the dark region (left, solid), the swirl region (central, dashed), and the active region (right, dot–dashed) at CML = 117, 160, 220, and 244°. The eastern end of the dark region appears dotted where it is not sharply defined. The latitude/longitude grid has a 10° spacing, the CML is marked with a vertical dashed line, and the λ_{III} = 180° meridian is indicated with another dashed line. Dots indicate magnetic local noon mapped from 15 R_J using the VIP4 model. At the time of going to press a colour version of this figure was available for download from http://www.cambridge.org/9780521035453.

solar wind in this case is principally to determine the size of the cavity within which the plasma rotation takes place, such that the principal modulating parameter will be the solar wind dynamic pressure. As pointed out independently by both Cowley and Bunce (2001) and Southwood and Kivelson (2001), the sense of the dependence will be one of anti-correlation. The basic argument is simply stated. When the solar wind dynamic pressure is low, the magnetosphere will be expanded, the plasma angular velocities low, the currents high, and the auroral emissions bright. Conversely, when the dynamic pressure is high, the magnetosphere will be compressed, the plasma angular velocities high, the currents low, and the auroral emissions dim. Furthermore, the latitude of the auroral emissions is not expected to change significantly, since uniform compressions and expansions of the magnetosphere do not change the positions of the feet of middle magnetosphere field lines in the ionosphere. Future observations are required to establish whether or not these expectations are fulfilled. The results of some initial studies have been discussed in Section 26.1.12, which indicate positive correlations between solar wind dynamic pressure and main oval auroral intensity. For example, during the *Cassini* flyby in December 2000, Gurnett *et al.* (2002) found a transient (few hour) UV auroral brightening to occur during an interval of solar wind compression. However, these observations do not indicate in which component of the aurora these changes took place, and it is possible to suggest a number of mechanisms that could lead to transient brightening poleward of the main oval under these conditions, such as shock-induced changes in solar wind coupling at the magnetopause. It should also be emphasized that the expected anti-correlation in the main oval emission discussed here is not transient in nature, but should persist on long timescales during compression and expansion events. Future study of more complete and well-determined data sets is required to elucidate these issues, and to resolve the various processes that may be occurring.

26.4 JUPITER'S POLAR AURORA

Jupiter's polar auroral emissions are of great interest, in part because they are the most highly variable, and in part because their mapping to Jupiter's outer magnetosphere implies that they should be the most Earth-like of the auroral processes active at Jupiter. These emissions vary independently of (and much more rapidly than) the

satellite footprint and main oval auroral emissions, and they appear to lag well behind corotation with Jupiter's magnetic field. From their observed high latitudes they must map to distant regions of the magnetosphere, ~30 R_J to open field lines, which is consistent with the subcorotational motions. They exhibit generally strong local time effects, as expected for distant regions of the magnetosphere. They are thought to reflect physical processes in regions of Jupiter's middle and outer magnetosphere, which may well be distinct from the processes responsible for the other emissions.

The middle and outer magnetosphere are regions where the plasma is in only partial corotation, but the plasma motions are still predominantly in the rotational direction. The influence of the solar wind pressure leads to characteristic local time dynamical motions of the plasma and distortions of the magnetic field. The polar auroral emissions provide a projection of these energetic processes, however, the magnetic mapping from Jupiter to these regions is highly uncertain. The dominance of the current sheet to the magnetic field in the middle and outer magnetosphere makes it difficult to know where a particular auroral emission maps without simultaneous measurements of the current sheet. This means that one can identify auroral processes within the polar regions and their characteristics (locations and motions, characteristic energies, variations with time, etc.), but in practice one can only generally identify the regions in the magnetosphere giving rise to these auroral processes. Within this constraint, in this section the observed properties of the polar aurora will be discussed, with some general inferences about the physical processes in the magnetosphere which may drive these aurora.

26.4.1 Overview of Polar Emissions

The presence of diffuse emissions poleward of the main oval was first detected in UV images with the FOC, primarily in the dusk half of the northern main oval (Gérard *et al.* 1994a). While the observing geometry for the southern aurora is not as favorable as in the north, similar regions appear to be present at conjugate points in the south. The following discussion will concentrate on the northern emission regions. The northern diffuse emissions were at first interpreted as a dawn/dusk asymmetry, but with images over a limited range of longitudes it was not clear to what extent these features were actually fixed in local time. WFPC2 images (Clarke *et al.* 1995, Ballester *et al.* 1996) confirmed the presence of patchy regions of emission in that sector, along with a generally broken main oval structure. Simulations of the auroral morphology (Satoh *et al.* 1996, Grodent *et al.* 1997, Pallier and Prangé 2001) suggest that these diffuse emissions may result from multiple arcs and broad diffuse emission at longitudes $120° < \lambda_{III} < 180°$. Infrared H_3^+ images also showed emissions from a region poleward of the main oval (Satoh and Connerney 1999). This region is filled with weak emission and contains significant local-time enhancements to the emission levels. This IR enhancement has been modeled with a "Yin-Yang" shape, with the polar region split into two segments of equal area:

- An IR bright region characterized by local-time enhancements in the dusk side, this feature has a terrestrial analog attributed to enhanced Joule heating of the Earth's ionosphere and overlaps the UV "active region" (discussed below).
- A less IR bright emission region in the dawn side, corresponding to the UV dark and swirl regions (discussed below).

The high resolution and high sensitivity UV images taken with STIS (Figure 26.1) reveal the full distribution and timescales for variations of the polar auroral emissions. It is difficult to determine the degree of corotation of discrete emissions in the polar regions due to their short lifetimes. However, features persisting long enough to permit an estimate have appeared to be moving at ~1/2 the corotation speed (Grodent *et al.* 2003b), consistent with a mapping to the outer magnetosphere. A statistical analysis of the UV polar emissions indicates that the northern polar region may be divided into three overlapping subregions, showing different average brightnesses and dynamical behaviors. The *dark region* (solid contour), the *swirl region* (dashed contour), and the *active region* (dot-dash contour) are outlined at a range of CML values in Figure 26.16. Further evidence for the source region for the polar aurora comes from comparison with the theoretical location of Ganymede's magnetic footprint from the VIP4 model, which can be used to indicate the magnetic noon meridian (at 15 R_J). In comparison with this landmark overlaid in Figure 26.16 as a dot, the three polar regions are seen to be fixed in magnetic local time (MLT). This implies that they are magnetically connected to magnetospheric processes occurring at fixed local times, also consistent with processes in the outer magnetosphere.

The *dark region* (in the north) is a crescent shaped region almost devoid of auroral emissions in the dawn sector (solid contour in Figure 26.16). The upper limit to auroral emissions is a few kR, almost equal to the airglow level away from the polar regions. The dark region is limited by the main oval on the equatorward edge and by the swirl and active regions, described below, on the poleward edge. An observer above the north pole (fixed relative to the direction of the Sun) would see the dark region confined to the dawn to noon sector as the CML increases from 110° to 270°. The dark region appears to be stretched in longitude parallel to the main oval. At λ_{III} CML < 180° (upper panels of Figure 26.16), the dotted portion of the solid contour is not sharply defined and depends on the emission gradient between the equatorward edge of the active region and the dusk portion of the main oval. In images with λ_{III} CML > 180° the active region is more easily observed, and it provides a sharper boundary for the eastern end of the dark region. This is nearly fixed relative to the magnetic noon meridian, implying a region fixed in MLT. The UV dark region may be identified with the rotating Dark Polar Region (r-DPR) deduced from ground-based Doppler IR observations (Stallard *et al.* 2001, 2003), which is also adjacent to the poleward edge of the main oval in the dawn sector. The ionospheric plasma within the IR region has been found to flow sunward at subcorotational speeds.

The northern *swirl region* (dashed contour in Figure 26.16) displays faint, patchy, and short lived (tens of seconds) emissions, characterized by turbulent motions that appear to swirl and fill approximately one third of the central

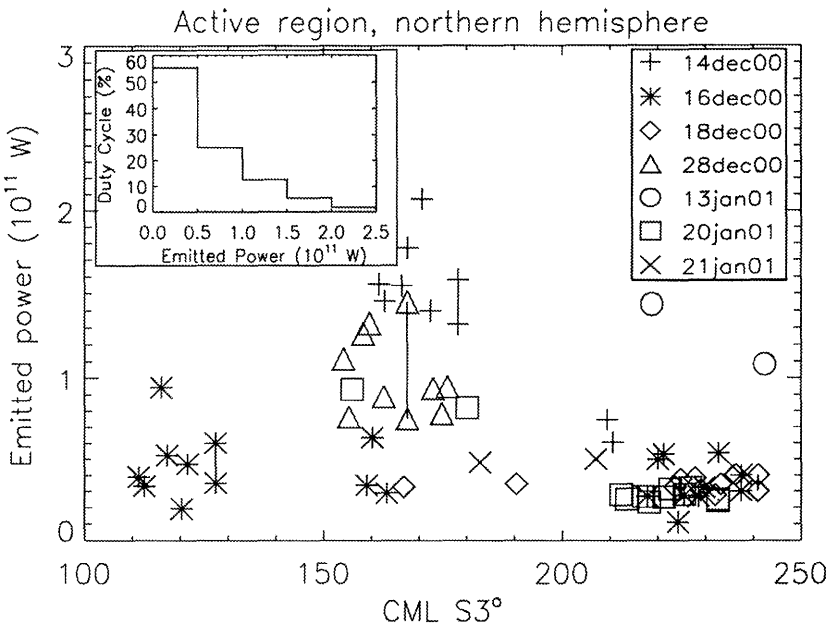

Figure 26.17. Plot of power in the active region versus CML over December 2000–January 2001 (Grodent *et al.* 2003b). There is evidence for a concentration when the active region is near local noon, however, there is a strong observational bias which has not been removed. The inset shows the distribution of emitted power for this region, indicating the duty cycle for auroral flares in the active region.

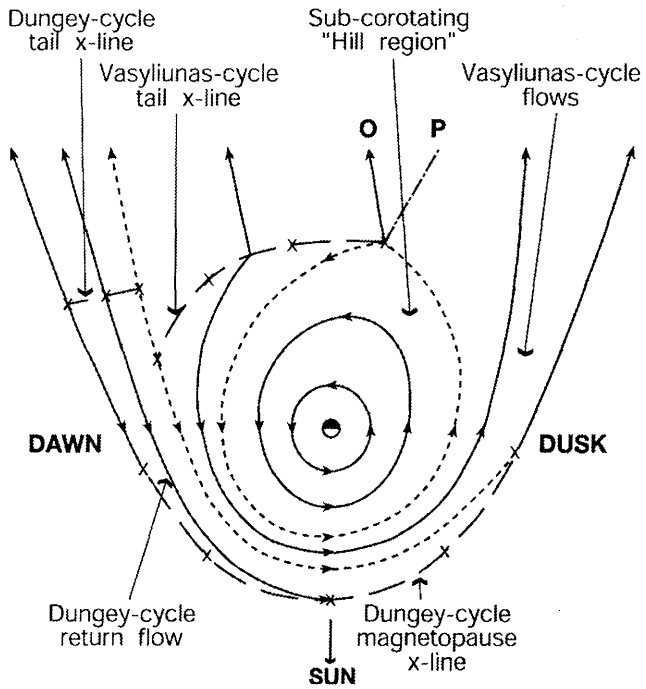

Figure 26.18. Sketch of the plasma flows in the jovian equatorial plane, where the direction to the Sun is at the bottom of the diagram, dusk is to the right, and dawn to the left. Arrowed solid lines show plasma streamlines, arrowed short-dashed lines show the boundaries between flow regimes (also streamlines), and the long-dashed lines with X's show the reconnection X-lines. O marks the path of the plasmoid O-line in the Vasyliunas-cycle flow (also a streamline), while P marks the outer boundary of the plasmoid.

area limited by the main oval. On average, this region contributes half of the total polar UV emission. It is variable, ranging from 0 to 200 kR above the planetary disk background. Its dawn to noon flank is clearly limited by the poleward edge of the dark region, while the noon to dusk flank is partially limited by the active region. In the latter sector, the upper panels of Figure 26.16 show that the swirl and active regions overlap when λ_{III} CML $< 180°$. The discrimination between the different regions rests not only on the different morphologies but also on the dynamical behaviors observed in image sequences and time tagged images. At higher CMLs (lower panels of Figure 26.16) the active region appears shifted equatorward and the two regions are better discriminated, though some overlap remains. The location and shape of the UV swirl region matches well the IR fixed Dark Polar Region (f-DPR) observed by Stallard *et al.* (2003) which is described as a region in which the plasma is near-stagnant in a reference frame oriented with respect to the Sun but fixed to the rotating magnetic pole.

The *active region* includes the remaining emission from the polar regions. This region appears to be confined to the noon to post-noon sector (Pallier and Prangé 2001). Bright localized transient events, the "polar flares", are occasionally observed in this region. These flares, along with the dawn storms, are the brightest auroral emissions observed from Jupiter, exceeding 10 MR for brief periods. Bright emissions that may be related to polar flares have been reported in FOC images since 1992 (Pallier and Prangé 2001). Afterward, similar bright emissions were detected with a growing sensitivity and spatial resolution with WFPC2 (Clarke *et al.* 1998). In 1999 an extremely bright polar flare was observed with high time resolution by STIS (Waite *et al.* 2001). The flare began as a small "pinpoint" emisssion near $\lambda_{III} = 167°$ longitude and 63° N. It brightened rapidly, reaching a maximum brightness of 37 MR in about 70 s. This abrupt

rise was followed by an exponential decline over a few minutes. For this event it was speculated that a sharp jump in the dynamic pressure at Jupiter's dayside magnetopause may have produced the disturbance that manifested itself in the polar flare. Extending the identification of the UV and IR regions suggests that the IR Bright Polar Region (BPR) described by Stallard *et al.* (2001, 2003) overlaps the active region.

The strong variability of the flares does not appear consistent with a slower solar wind controlled process, as would be expected if the flaring emissions were filling the polar cusp region. Instead, these rapid events may be a signature of a sporadic reconnection with the IMF at the dayside magnetopause. While it seems increasingly likely that the bright auroral features (flares) discussed above are magnetically connected to the boundary of the dayside magnetosphere, little has been said about jovian dayside reconnection. Analysis of *Voyager* data during entry into the jovian magnetosphere (Huddleston *et al.* 1997) revealed bursty reconnection phases, with the IMF characterized by flux transfer event (FTE) structures with timescales less than one minute. It was suggested that if the IMF direction is at a favorable angle to the magnetospheric field, sudden dynamic pressure jumps could lead to bursty reconnection events, allowing solar wind momentum to be transmitted into the magnetosphere. Walker and Russell (1985) found 14 possible FTEs in the *Pioneer 10* and *11* and *Voyager 1* and *2* observations of the jovian magnetic field. Most of them were less than 1 min in duration and four of them were separated by about 4 min. These timescales are in agreement with the characteristic times of the flaring emissions observed in the FUV images.

A statistical analysis of the northern dataset shows that the active region always exhibits auroral emission, but with a highly variable intensity. Figure 26.17 displays the power emitted in the active region as a function of CML from day to day during the *Cassini* flyby campaign. The histogram plotted in the upper left corner of Figure 26.17 shows the percent of time the active region emissions, averaged over the exposure time, are in a given power range. It appears that for almost 55% of the observing time the emission was between 0 and 0.5×10^{11}W, and it exceeded 1.5×10^{11}W about 7% of the time. During this campaign the probability for observing a relatively bright auroral flare ($\geq 1.5 \times 10^{11}$ W) in the north was less than 10%, while there was a 30% chance to observe a moderate flare ($0.5\text{–}1.5 \times 10^{11}$ W). The analysis of spectral observations obtained with STIS (Gérard *et al.* 2003) shows that the electron energies in the polar flares ranged from 40 to 120 keV in their observations, close to the values in the main oval. The time evolution of this energy shows little correlation or anticorrelation with the energy flux precipitated during these transient events. Gérard *et al.* (2003) suggest that, compared to the main auroral oval emission, the mechanism responsible for the flares did not increase the energy of the precipitated electrons but it enhanced their number flux.

High spatial resolution observations made with the Chandra X-ray Observatory (Gladstone *et al.* 2002) demonstrate that most of Jupiter's northern auroral X-rays come from a hot spot located in a narrow region limited by $\lambda_{III} = 160\text{–}180°$ and latitudes = 60–70°, and modulated with a ~40 min periodicity. Simultaneous STIS images show

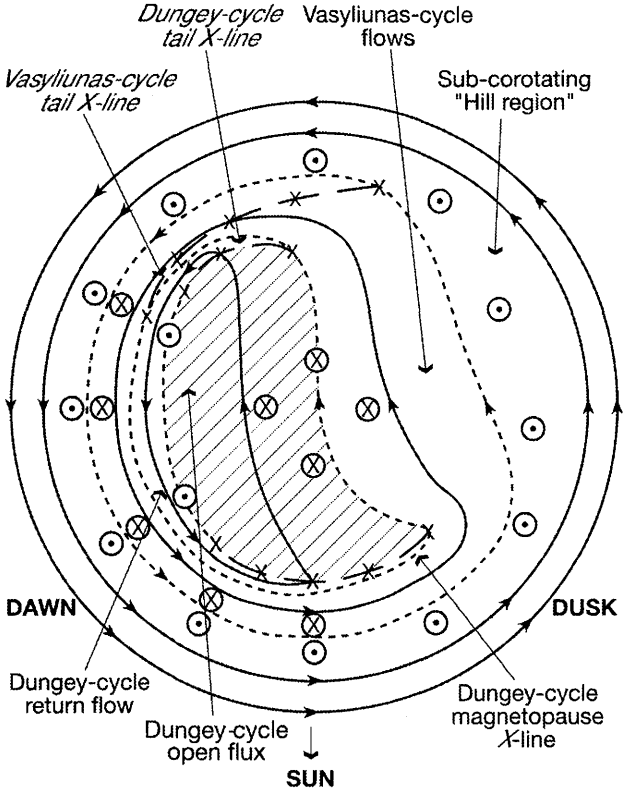

Figure 26.19. Sketch of the plasma flows in the northern jovian ionosphere in a format similar to Figure 26.18, where the direction to the Sun is at the bottom of the diagram, dusk is to the right, and dawn to the left. The region of Dungey-cycle open flux is shown hatched. Circled dots and crosses indicate regions of upward and downward field-aligned current, respectively. Field-perpendicular Hall currents flow generally anticlockwise round the pole, while Pedersen currents flow generally equatorward.

that the X-ray photons are superimposed on a series of UV spots appearing inside the active region. The same precipitating particles could be responsible for both emissions. It has been suggested that either sulfur and oxygen ions originating from the Io plasma torus or bremsstrahlung emission from precipitating electrons could give rise to such polar X-ray emissions (Waite *et al.* 1994, Maurellis *et al.* 2000). Another explanation consistent with the distant mapping of these emissions invokes high latitude reconnection of the planetary and solar wind magnetic fields, with the subsequent entry of the highly ionized heavy ion component of the solar wind. The captured ions would then be accelerated by field-aligned potentials present in the outer magnetosphere, and precipitated into the loss cone (Gladstone *et al.* 2002).

26.4.2 Distorted Structure in the Northern Aurora

An apparent motion of one segment of the northern aurora over $80° \leq \lambda_{III} \leq 140°$ from within the polar regions down to the presumed latitude of the main oval has been reported from WFPC2 images (Ballester *et al.* 1996, Clarke *et al.* 1998). This "equatorward surge" appeared to occur systematically during each rotation as this region moved from local noon to evening. The equatorward surge is also observed in

STIS images, but with higher signal to noise the motion appears more complicated. The equatorward motion is accompanied by a subcorotation "slippage" of the arc. This motion might be regarded as the ionospheric counterpart of the compression of the dayside magnetosphere, squeezing and accelerating the plasma. Stallard *et al.* (2001) discussed banded IR and UV auroral emissions observed poleward of the main oval, and suggested that they are produced by a stepwise breakdown in corotation of the equatorial plasma. Such a description implies that a considerable portion of the polar region is still under the control of field lines that are closed and connecting to the middle magnetosphere. An alternate explanation compatible with the surge and an overlapping with the polar flares would be that the arc-like feature results from disturbances occurring at the dayside magnetopause.

While in individual images the main oval may appear at varying latitudes (Pallier and Prangé 2001), in a statistical average image the main oval appears clearly defined with a "kinked" shape in the range $80° \leq \lambda_{III} \leq 140°$ (Figure 26.10). The general structure of the kink is fixed in System III (it appears to be the same in images taken at different CML values), and *Galileo* partly imaged it on the nightside (Vasavada *et al.* 1999). Since the distortion in this region rotates with Jupiter, it is not due to local time effects. The combined observations that this feature is fixed with respect to Jupiter, that it is unchanged over several years time, that it appears in the north but not at conjugate locations in the south, and that the separation of the satellite footprints from the main oval increases in this range, are all consistent with a source internal to Jupiter and corresponding to an anomalously weak magnetic field (Clarke *et al.* 2002b). The possibility of a "magnetic anomaly" in this region of Jupiter's magnetic field deserves further analysis. It has been suggested on theoretical grounds (Dessler 1983) and would generally be consistent with a large number of prior observations of "pulsar-like" modulations of various jovian emissions. If confirmed, it is proposed that this feature be known as the "Dessler anomaly".

26.4.3 Theory of the Polar Aurora

Theoretical discussion of the aurora poleward of the main oval, and its origins in processes beyond the middle magnetosphere, is currently at an early stage of development. Nevertheless, some comments will be offered here based on the simple conceptual picture presented by Cowley *et al.* (2003b). Figure 26.18 shows a view of the flow in the jovian equatorial plane following the discussion of Cowley *et al.* (1996), where the direction to the Sun is at the bottom of the figure, dawn is to the left and dusk to the right. Three elements of the flow are identified. The first is an inner region of the middle magnetosphere where the plasma streamlines form closed paths around the planet, though extending to greater distances on the nightside than on the dayside in accordance with the day–night asymmetry in the current sheet field (Bunce and Cowley 2001a, Khurana 2001). The angular velocity of the outwardly diffusing iogenic plasma falls increasingly from rigid corotation with increasing distance in this region, as first described by Hill (1979) (and as discussed above in the main oval section). For this reason the region is labeled "subcorotating Hill region" in Figure 26.18.

The Hill region is then surrounded by a region, still driven by planetary rotation, in which the dynamics of the middle magnetosphere current sheet play an important role in the loss of iogenic plasma down-tail. As first discussed by Vasyliunas (1983), it is envisioned that outer current sheet flux tubes that are confined by the solar wind on the dayside, flow down-tail away from the planet as they rotate into the dusk sector. The anti-sunward-flowing distended flux tubes eventually pinch off via magnetic reconnection within the current sheet, forming "plasmoids" consisting of closed loops of magnetic flux, which flow down-tail in the dusk and midnight sector of the magnetotail. The resulting equatorial flow pattern (following Vasyliunas 1983) is shown for simplicity in Figure 26.18 as a steady-state process, though recent observations indicate considerable time-dependency (Woch *et al.* 2002). The reconnection line associated with the formation of the plasmoid is indicated by the nightside dashed line marked X. The location of the outer edge of the plasmoid is then indicated by the dot–dashed line marked P (which eventually asymptotes to the dusk magnetopause), while the central O-type line of the plasmoid (a streamline) is indicated by O. The sense of the equatorial magnetic field thus points out of the plane of the diagram, opposite to the sense of the internal planetary field, tailward of the Vasyliunas-cycle X-line and dawnward of the O-line. We thus anticipate that the central Hill region will be surrounded by somewhat faster sunward-flowing (but still subcorotating) plasma-depleted flux tubes on the dawn side on streamlines that originate from the Vasyliunas-cycle X-line, while slowing again on the dusk side due to further mass-loading by outwardly diffusing iogenic plasma.

The third region is a layer on the dawn side of the planet in which flow is driven by interaction with the solar wind, specifically through reconnection between the planetary field and the interplanetary magnetic field (IMF) which is draped over the dayside magnetopause. As first discussed by Dungey (1961) for the case of the Earth, reconnection at the "Dungey-cycle magnetopause X-line" shown in Figure 26.19, which is favored for northward-directed IMF in the case of Jupiter, produces "open" flux tubes mapping from the planet's poles into the solar wind. These are then transported (out of the plane of the diagram) anti-sunward by the solar wind and are stretched into a long magnetic tail. The latter thus consists of two lobes of oppositely directed magnetic flux which map into the northern and southern poles of the planet, respectively. Reconnection between the lobe fields in the central plane of the tail at the "Dungey-cycle tail X-line" then returns closed flux tubes to the planet on one side of the X-line, while flux tubes which are disconnected from the planet flow anti-sunward back into the solar wind on the other. Because the dusk side of the tail is occupied by outward flowing iogenic plasma via the Vasyliunas cycle as just described, however, it is envisioned that the Dungey-cycle tail X-line will be confined to the dawn side of the tail as shown in Figure 26.18. The open flux tubes in the lobes thus flow inward and dawnward to the tail X-line, while the "return flow" of closed flux tubes is confined to an outer layer on the dawn side of the magnetosphere, as shown. This layer is identified with the "outer magnetosphere" field layer observed in spacecraft data, which overlies the middle magnetosphere current sheet fields on the dayside (e.g., Acuña *et al.* 1983).

This flow pattern is now mapped along magnetic field lines to the ionosphere, and the plasma flow in the rest-frame of the planetary dipole is shown schematically in Figure 26.19 (the pole is roughly in the center of the diagram). The circled dots and crosses indicate the presence of upward- and downward-directed field-aligned currents (FACs), respectively, associated with the divergence of the horizontal ionospheric current (principally the Pedersen current). In considering the latter, it should be remembered that the ionospheric current is determined by the electric field in the rest frame of the neutral atmosphere, and that to a first approximation this is rotating with the planet at an angular velocity which is greater than that of the generally subcorotating plasma. As a zeroth-order approximation, the plasma near-rigidly corotates at lower latitudes, but departs increasingly to lower angular velocities as the pole is approached. This gives rise to an equatorward-directed electric field in the rest frame of the neutral atmosphere where the plasma departs from rigid corotation, and hence an equatorward-directed Pedersen current throughout the high-latitude region. Continuity of this current then requires generally downward-directed FAC in the central region near the pole, and upward-directed FAC at lower latitudes. The Hall current then flows generally anticlockwise around the pole, carried by collision-dominated ions flowing with the neutral atmosphere in the lower ionosphere.

The flow and current shown in Figure 26.19 are now considered in more detail. In the outer part of the diagram, near-rigid corotating flow at the lowest latitudes shown gives way with increasing latitude to subcorotation and upward-directed FAC in the Hill region, as just indicated. This upward-directed FAC has been suggested to be associated with the main oval auroral emissions in the main oval section. Poleward of this region one then has a region of subcorotating flow which is modulated in local time by the Vasyliunas cycle, being faster on the dawn side downstream from the mapped Vasyliunas-cycle X-line, where the equatorward ionospheric currents will therefore be weaker, and slower on the dusk side, where the ionospheric currents will therefore be stronger. The faster (less subcorotational) flows on the dawn side may then lead to a reversal in the FAC to downward-directed in this sector, in the region poleward of the Hill region as shown in Figure 26.19, and as inferred from spacecraft data by both Bunce and Cowley (2001b) and Khurana (2001). This region of downward current may be expected to be aurorally dark, leading to a main oval that is latitudinally confined in the dawn sector, more so than at dusk where the upward current may be more distributed, extending into the region of Vasyliunas-cycle flows. In addition, time-dependent current sheet activity (i.e., plasmoid formation) may also occur in the latter region at dusk, leading to smaller scale time-dependent subcorotating flow and precipitation structures associated with these dynamics.

At the highest latitudes one then has a region of open magnetic flux associated with the Dungey cycle, indicated by the hatched region in Figure 26.19. This is shown roughly symmetrically located with respect to noon on the dayside where the field lines map to the magnetopause reconnection sites, but is skewed towards dawn on the nightside due to the Vasyliunas-cycle tail outflow in the dusk sector as discussed above. The flow in the region of open tubes is predominantly anti-sunward and modulated by the direction of the IMF (which governs the rate of reconnection at the dayside magnetopause), but is expected generally to be very slow. Simple estimates indicate transit times of open flux tubes through the tail lobes, and hence across the region of open flux in the ionosphere, of several days, associated with flow speeds of $\sim$100 m s^{-1} or less. This region will therefore be semi-stagnant in comparison with the general subcorotating flows ($\sim$1–2 km s^{-1}) of surrounding regions. This open region may also be expected to be dark in respect to the UV auroral emissions. The return flow of the Dungey cycle is confined to a thin layer on the dawn side of the region of open flux, in conformity with the equatorial flow shown in Figure 26.17, thus giving rise to single-cell ionospheric flow, as opposed to the twin-cell flow excited by the Dungey cycle at Earth.

Relating this theoretical discussion to the observations, Cowley *et al.* (2003) suggested that the subcorotating IR r-DPR, and the overlapping UV dark region, may plausibly be connected with the partially-emptied flux tubes and downward-directed FACs in the dawn side sunward return flows associated with the Dungey and Vasyliunas cycles. They also suggested that the semi-stagnant IR f-DPR region, which appears to overlap at least the dawnward part of the UV swirl region, poleward of the active region, corresponds to the region of open flux mapping to the tail lobes which is associated with the solar wind-driven Dungey cycle (hatched region in Figure 26.19). The issue of the origins of both the IR and UV emission in this region, however, remains open. The IR BPR then appears to correspond to the UV active region in the noon sector, and possibly also to a portion of the swirl region closer to dusk. The latter region corresponds to the down-tail flow of the Vasyliunas cycle in the theoretical picture in Figure 26.19, in conformity with the IR Doppler observations of subcorotational anti-sunward flow in this region. The active region is then suggested to be connected with the dayside magnetopause and boundary layers, where reconnection events between the jovian field and the IMF initiate the Dungey cycle, corresponding to "flux transfer events" at Earth. Similarly, transient events in the nightside reconnection regions may then give rise to the "dawn storm" phenomenon, corresponding to substorms at Earth. Further and more detailed observations should be able to test this proposed theoretical interpretation of Jupiter's polar aurora.

26.5 SUMMARY

The state of observations of Jupiter's aurora has advanced greatly over the past 25 years, starting with its discovery and extending to multiple wavelengths and high sensitivity and resolution. In fact, present day HST images of Jupiter's UV aurora have higher resolution as a fraction of the planet's diameter than images of the Earth's aurora from orbital instruments. These studies of Jupiter have revealed the high degree of complexity of Jupiter's auroral processes, for example showing the three apparently independent auroral regions. Jupiter's magnetosphere, ionosphere, and aurora are coupled processes, forming a giant electromagnetic circuit around the planet. In situ measurements of Jupiter's magnetospheric charged particles and fields, combined at times with coordinated remote observations, have provided unique

and invaluable information toward understanding the nature of these coupled processes. Comparison with theoretical constructs and computer models may further advance efforts to place the auroral and magnetospheric processes on a firm physical basis. At this time, it appears that the basic auroral emissions, their distributions, and their spectral and energetic properties have been identified. The following questions, however, remain to be answered:

- What magnetospheric processes in general trigger the precipitation of auroral particles at Jupiter?
- What are the specific causes of Jupiter's main oval, the satellite footprints, and the polar emissions?
- Where are the magnetospheric sources of the polar flares and the dawn storms, and what physical processes lead to these auroral storms?
- How are Jupiter's auroral processes similar to Earth's and how to they differ?
- Which processes in Jupiter's magnetosphere are influenced by the solar wind and which processes are controlled by Io?
- What is the impact of auroral processes on Jupiter's upper atmosphere?

Given the many different timescales for variability, future progress in understanding this coupled system may require much more complete and coordinated measurements of the auroral emissions with other properties of the jovian system. Examples include measurements of the aurora coordinated with measurements of Io's volcanic activity, Io's atmosphere, the density and temperature of the plasma torus, the distribution, energy, and dynamics of the magnetospheric plasma, the properties of the impinging solar wind, and the dynamics and energetics of Jupiter's upper atmosphere. It is through such coupled measurements with higher duty cycles that we can hope to gain understanding of this coupled physical system.

Acknowledgements. The authors would like to thank Jean-Claude Gérard, Tom Hill, Renée Prangé, and Nick Schneider for helpful comments in the course of writing this chapter. EJB was supported during the course of this study by PPARC Grant PPA/G/O/2001/00014, SWHC by PPARC Senior Fellowship PPA/N/S/2000/00197, and DG by the Belgian Fund for Scientific Research (FNRS).

REFERENCES

Achilleos, N., S. Miller, J. Tennyson, A. D. Aylward, I. Mueller-Wodarg, and D. Rees, JIM: A time-dependent, three-dimensional model of Jupiter's thermosphere and ionosphere, *J. Geophys. Res.* **103**, 20 089–20 112, 1998.

Acuña, M. H., F. M. Neubauer, and N. F. Ness, Standing Alfvén wave current system at Io: *Voyager 1* observations, *J. Geophys. Res.* **86**, 8513–8522, 1981.

Acuña, M. H., J. E. P. Connerney, and K. W. Behannon, Magnetic field and magnetosphere, in *Physics of the Jovian Magnetosphere*, A. J. Dessler (ed.), Cambridge University Press, pp. 1–50, 1983.

Ajello, J., D. Shemanksy, W. Pryor, K. Tobiska, C. Hord, S. Stephens, I. Stewart, J. Clarke, K. Simmons, W. McClintock, C. Barth, J. Gebben, D. Miller, and B. Sandel, *Galileo* orbiter ultraviolet observations of Jupiter aurora, *J. Geophys. Res.* **103**, 20 125–20 148, 1998.

Bagenal, F., Alfvén wave propagation in the Io plasma torus, *J. Geophys. Res.* **88**, 3013, 1983.

Bagenal, F., Empirical model of the Io plasma torus: *Voyager* measurements, *J. Geophys. Res.* **99**, 11 043–11 062, 1994.

Ballester *et al.*, G. E., Time-resolved observations of Jupiter's far-ultraviolet aurora, *Science* **274**, 409–413, 1996.

Barbosa, D. D., Dynamics of field-aligned current sources at Earth and Jupiter, in *Magnetospheric Currents*, T. A. Potemra (ed.), AGU, p. 350, 1983.

Baron, R., R. D. Joseph, T. Owen, J. Tennyson, S. Miller, and G. E. Ballester, Imaging Jupiter's aurorae from H_3^+ emissions in the 3–4 μm band, *Nature* **353**, 539–542, 1991.

Baron, R., T. Owen, J. Connerney, T. Satoh, and J. Harrington, Solar wind control of Jupiter's H_3^+ aurorae, *Icarus* **120**, 437–442, 1996.

Barrow, C. H. and M. D. Desch, Solar wind control of Jupiter's hectometric radio emission, *A&A* **213**, 495–501, 1989.

Barrow, C. H., M. D. Desch, and F. Genova, Solar wind control of Jupiter's decametric radio emission, *A&A* **165**, 244–250, 1986.

Bauske, R., M. R. Combi, and J. T. Clarke, Analysis of midlatitude auroral emissions observed during the impact of Comet Shoemaker–Levy 9 with Jupiter, *Icarus* **142**, 106–115, 1999.

Belcher, J. W., The Jupiter–Io connection: An Alfvén engine in space, *Science* **238**, 170–176, 1987.

Bhardwaj, A. and G. R. Gladstone, Auroral emissions of the giant planets, *Rev. Geophys.* **38**, 295–353, 2000.

Bhardwaj, A., G. R. Gladstone, and P. Zarka, An overview of Io flux tube footprints in Jupiter's auroral ionosphere, *Adv. Space Res.* **27**, 1915–1922, 2001.

Bigg, E. K., Influence of the satellite Io on Jupiter's decametric emission, *Nature* **203**, 1008–1010, 1964.

Broadfoot, A. L., M. J. S. Belton, P. Z. Takacs, B. R. Sandel, D. E. Shemansky, J. B. Holberg, J. M. Ajello, S. K. Atreya, T. M. Donahue, H. W. Moos, J. L. Bertaux, J. E. Blamont, D. F. Strobel, J. C. McConnell, A. Dalgarno, R. Goody, and M. B. McElroy, Extreme ultraviolet observations from *Voyager 1*: Encounter with Jupiter, *Science* **204**, 979–982, 1979.

Brown, R. A., A model of Jupiter's sulfur nebula, *ApJ* **206**, L179–L183, 1976.

Bunce, E. J. and S. W. H. Cowley, Local time asymmetry of the equatorial current sheet in Jupiter's magnetosphere, *Planet. Space Sci.* **49**, 261–274, 2001a.

Bunce, E. J. and S. W. H. Cowley, Divergence of the equatorial current in the dawn sector of Jupiter's magnetosphere: Analysis of *Pioneer* and *Voyager* magnetic field data, *Planet. Space Sci.* **49**, 1089–1113, 2001b.

Bunce, E. J., P. G. Hanlon, and S. W. H. Cowley, A simple empirical model of the equatorial radial field in Jupiter's middle magnetosphere, based on spacecraft fly-by and *Galileo* orbiter data, *Planet. Space Sci.* **50**, 789–806, 2002.

Burke, B. F. and K. L. Franklin, Observations of a variable radio source associated with the planet Jupiter, *J. Geophys. Res.* **60**, 213–217, 1955.

Caldwell, J., A. T. Tokunaga, and F. C. Gillett, Possible infrared aurorae on Jupiter, *Icarus* **44**, 667–675, 1980.

Caldwell, J., H. Halthore, G. Orton, and J. Bergstralh, Infrared polar brightenings on Jupiter: IV. Spatial properties of methane emission, *Icarus* **74**, 331–339, 1988.

Caldwell, J., B. Turgeon, and X. Hua, Hubble Space Telescope imaging of the north polar aurora on Jupiter, *Science* **257**, 1512–1515, 1992.

Carr, T. D. and F. Reyes, Microstructure of jovian decametric S bursts, *J. Geophys. Res.* **104**, 25 127–25 141, 1999.

Carr, T. D., M. D. Desch, and J. K. Alexander, Phenomenology of magnetospheric radio emission, in *Physics of the jovian Magnetosphere*, A. J. Dessler (ed.), Cambridge University Press, pp. 226–284, 1983.

Caudal, G., A self-consistent model of Jupiter's magnetodisc including the effects of centrifugal force and pressure, *J. Geophys. Res.* **91**, 4201–4221, 1986.

Chamberlain, J. W. and D. M. Hunten, *Theory of Planetary Atmospheres: An Introduction to Their Physics and Chemistry*, Academic Press, New York, 1987.

Clarke, J. T., HST observations of Jupiter's UV aurora, in *A Decade of Hubble Space Telescope Science*, M. Livio, K. Noll, and M. Stiavelli (Eds.), Cambridge Univ. Press, 25, 2003.

Clarke, J. T., H. W. Moos, S. K. Atreya, and A. L. Lane, Observations from Earth orbit and variability of the polar aurora on Jupiter, *ApJ* **241**, L179–L182, 1980.

Clarke, J. T., J. Trauger, and J. H. Waite, Doppler-shifted H Lyman-α emission from Jupiter's aurora, *Geophys. Res. Lett.* **16**, 587–590, 1989.

Clarke, J. T., G. Ballester, J. Trauger, K. T. J. Ajello, W. Pryor, J. E. P. Connerney, G. R. Gladstone, J. H. Waite Jr., L. B. Jaffel, and J.-C. Gérard, Hubble Space Telescope imaging of Jupiter's UV aurora during the *Galileo* orbiter mission, *J. Geophys. Res.* **103**, 20 217–20 236, 1998.

Clarke, J. T., J. Ajello, G. Ballester, L. B. Jaffel, J. Connerney, J.-C. Gérard, G. R. Gladstone, D. Grodent, W. Pryor, J. Trauger, and J. H. Waite, Ultraviolet auroral emissions from the magnetic footprints of Io, Ganymede, and Europa on Jupiter, *Nature* **415**, 997–1000, 2002a.

Clarke, J. T., D. Grodent, and J. E. P. Connerney, The distorted shape of Jupiter's northern auroral oval: A possible magnetic anomaly, *BAAS* **34**, 906, 2002b.

Clarke J. T. *et al.* , Hubble Space Telescope Goddard High Resolution Spectrograph H_2 rotational spectra of Jupiter's aurora, *ApJ* **430**, L73–L76, 1994.

Clarke J. T. *et al.*, Hubble Space Telescope far-ultraviolet imaging during the impacts of Comet Shoemaker–Levy 9, *Science* **267**, 1302–1307, 1995.

Clarke J. T. *et al.*, Far-UV imaging of Jupiter's aurora with HST WFPC 2, *Science* **274**, 404–409, 1996.

Connerney, J. E. P., Doing more with Jupiter's magnetic field, in *Planetary Radio Emissions III*, H. O. Rucker and S. J. Bauer, eds, pp. 13–33, Austrian Academy of Sciences Press, 1992.

Connerney, J. E. P., Magnetic fields of the outer planets, *J. Geophys. Res.* **98**, 18 659–18 679, 1993.

Connerney, J. E. P. and T. Satoh, The H_3^+ ion: A remote diagnostic of the jovian magnetosphere, *Phil. Trans. Roy. Soc. A.* **358**, 2471, 2000.

Connerney, J. E. P., M. H. Acuña, and N. F. Ness, Modeling the jovian current sheet and inner magnetosphere, *J. Geophys. Res.* **86**, 8370–8384, 1981.

Connerney, J. E. P., R. L. Baron, T. Satoh, and T. Owen, Images of excited H_3^+ at the foot of the Io flux tube in Jupiter's atmosphere, *Science* **262**, 1035–1038, 1993.

Connerney, J. E. P., T. Satoh, and R. L. Baron, Interpretation of auroral 'lightcurves' with application to jovian H_3^+ emissions, *Icarus* **122**, 24–35, 1996.

Connerney, J. E. P., M. H. Acuña, N. F. Ness, and T. Satoh, New models of Jupiter's magnetic field constrained by the Io flux tube footprint, *J. Geophys. Res.* **103**, 11 929–11 939, 1998.

Cowley, S. W. H. and E. J. Bunce, Origin of the main auroral oval in Jupiter's coupled magnetosphere–ionosphere system, *Planet. Space Sci.* **49**, 1067–1088, 2001.

Cowley, S. W. H., A. Balogh, M. K. Dougherty, M. W. Dunlop, T. M. Edwards, R. J. Forsyth, N. F. Laxton, and K. Staines, Plasma flow in the jovian magnetosphere and related magnetic effects: *Ulysses* observations, *J. Geophys. Res.* **101**, 15 197–15 210, 1996.

Cowley, S. W. H., J. D. Nichols, and E. J. Bunce, Distributions of current and auroral precipitation in Jupiter's middle magnetosphere computed from steady-state Hill–Pontius angular velocity profiles: Solutions for current sheet and dipole magnetic field models, *Planet. Space Sci.* **50**, 717–734, 2002.

Cowley, S. W. H., E. J. Bunce, and J. D. Nichols, Origins of Jupiter's main oval auroral emissions, *J. Geophys. Res.* **108**, 8002, 2003a.

Cowley, S. W. H., E. J. Bunce, T. S. Stallard, and S. Miller, Jupiter's polar ionospheric flows: Theoretical interpretation, *Geophys. Res. Lett.* **30**, 1220, 2003b.

Crary, F. J. and F. Bagenal, Coupling the plasma interaction at Io to Jupiter, *Geophys. Res. Lett.* **24**, 2135, 1997.

Delamere, P. A., F. Bagenal, R. E. Ergun, and Y.-J. Su, Momentum transfer between the Io plasma wake and Jupiter's ionosphere, *J. Geophys. Res.* **108**, 2003.

Desch, M. D. and M. L. Kaiser, Predictions for Uranus from a radiometric Bode's law, *Nature* **310**, 755–757, 1984.

Dessler, A. J. and J. W. Chamberlain, Jovian longitudinal asymmetry in Io-related and Europa-related auroral hot spots, *ApJ* **230**, 974–981, 1979.

Dessler, A. J. and T. W. Hill, Jovian longitudinal control of Io-related radio emissions, *ApJ* **227**, 664–675, 1979.

Dougherty, M. K., D. J. Southwood, A. Balogh, and E. J. Smith, Field-aligned currents in the jovian magnetosphere during the *Ulysses* flyby, *Planet. Space Sci.* **41**, 291–300, 1993.

Drossart, P., B. Bézard, S. K. Atreya, J. Lacy, E. Serabyn, A. Tokunaga, and T. Encrenaz, Enhanced acetylene emission near the north pole of Jupiter, *Icarus* **66**, 610–618, 1986.

Drossart, P., J. P. Maillard, J. Caldwell, S. J. Kim, J. K. G. Watson, W. A. Majewski, J. Tennyson, S. Miller, S. K. Atreya, J. Clarke, J. H. Waite Jr., and R. Wagener, Detection of H_3^+ on Jupiter, *Nature* **340**, 539–541, 1989.

Dungey, J. W., Interplanetary field and the auroral zones, *Phys. Rev. Lett.* **6**, 47–49, 1961.

Ellis, G. R. A., Observations of the Jupiter S bursts between 3.2 and 32 Mhz, *Aust. J. Phys.* **35**, 165–175, 1982.

Engle, I. M. and D. B. Beard, Idealized *Voyager* jovian magnetosphere shape and field, *J. Geophys. Res.* **85**, 579, 1980.

Feldman, P., M. A. McGrath, D. F. Strobel, H. W. Moos, K. D. Retherford, and B. C. Wolven, HST STIS ultraviolet imaging of polar aurora on Ganymede, *ApJ* **535**, 1085–1090, 2000.

Frank, L. A. and W. R. Paterson, Production of hydrogen ions at Io, *J. Geophys. Res.* **104**, 10 345–10 354, 1999.

Frank, L. A. and W. R. Paterson, *Galileo* observations of electrons beams and thermal ions in Jupiter's magnetosphere and their relationship to the auroras, *J. Geophys. Res.* **107**, 2002.

Frank, L. A., W. R. Paterson, K. L. Ackerson, V. M. Vasyliūnas, F. V. Coroniti, and S. J. Bolton, Plasma observations at Io with the *Galileo* spacecraft, *Science* **274**, 394, 1996.

Galopeau, P. H. M., M. Y. Boudjada, and H. O. Rucker, Efficiency of the cyclotron maser instability and occurrence probability of jovian decameter radio emissions, in *Planetary Radio Emissions V*, H. O. Rucker, M. L. Kaiser, and Y. Leblanc, eds, pp. 195–203, Austrian Academy of Sciences Press, 2001.

Gehrels, N. and E. Stone, Energetic oxygen and sulfur in the jovian magnetosphere and its contribution to auroral excitation, *J. Geophys. Res.* **88**, 5537–5550, 1983.

Geissler, P. E., A. S. McEwen, W. Ip, M. J. S. Belton, W. H. S. T. V. Johnson, and A. P. Ingersoll, *Galileo* imaging of atmospheric emissions from Io, *Science* **285**, 870–874, 1999.

Genova, F. and W. Calvert, The source location of jovian millisecond radio bursts with respect to Jupiter's magnetic field, *J. Geophys. Res.* **93**, 979–986, 1988.

Genova, F., P. Zarka, and C. H. Barrow, *Voyager* and Nançay observations of the jovian radio emission at different frequencies: Solar wind effect and source extent, *A&A* **182**, 159–162, 1987.

Gérard, J.-C., V. Dols, R. Prangé, and F. Paresce, The morphology of the north jovian ultraviolet aurora observed with

the Hubble Space Telescope, *Planet. Space Sci.* **42**, 905–917, 1994a.

Gérard, J.-C., D. Grodent, R. Prangé, J. H. Waite, G. R. Gladstone, V. Dols, F. Paresce, A. Storrs, L. B. Jaffel, and K. A. Franke, A remarkable auroral event on Jupiter observed in the ultraviolet with the Hubble Space Telescope, *Science* **266**, 1675–1678, 1994b.

Gérard, J.-C., J. Gustin, D. Grodent, P. Delamere, and J. T. Clarke, Excitation of the FUV Io tail on Jupiter: Characterization of the electron precipitation, *J. Geophys. Res.* **107**, 10.1029, 2002.

Gérard, J.-C., J. Gustin, D. Grodent, J. T. Clarke, and A. Grard, Spectral observations of transient features in the FUV jovian polar aurora, *J. Geophys. Res.* **in press**, 2003.

Gladstone, G. R., J. H. Waite Jr., D. Grodent, W. S. Lewis, F. J. Crary, R. F. Elsner, M. C. Weisskopf, T. Majeed, J.-M. Jahn, A. Bhardwaj, J. T. Clarke, D. T. Young, M. K. Dougherty, S. A. Espinosa, and T. E. Cravens, A pulsating auroral x-ray hot spot on Jupiter, *Nature* **415**, 1000–1003, 2002.

Goldreich, P. and D. Lynden-Bell, Io, a jovian unipolar inductor, *ApJ* **156**, 59–78, 1969.

Grodent, D., G. R. Gladstone, J.-C. G. an V. Dols, and J. H. Waite, Simulation of the morphology of the jovian UV north aurora observed with the Hubble Space Telescope, *Icarus* **128**, 306–321, 1997.

Grodent, D., J. H. Waite Jr., and J.-C. Gérard, A self-consistent model of the jovian auroral thermal structure, *J. Geophys. Res.* **106**, 12 933–12 952, 2001.

Grodent, D., J. T. Clarke, J. Kim, J. H. Waite Jr., and S. W. H. Cowley, Jupiter's main auroral oval observed with HST-STIS, *J. Geophys. Res.* **108**, 1387, 2003a.

Grodent, D., J. T. Clarke, J. H. Waite Jr., S. W. H. Cowley, J.-C. Gérard, and J. Kim, Jupiter's polar auroral emissions, *J. Geophys. Res.* **108**, 1366, 2003b.

Gurnett, D. A., W. S. Kurth, A. Roux, S. J. Bolton, and C. F. Kennel, *Galileo* plasma wave observations in the Io plasma torus and near Io, *Science* **274**, 391–392, 1996.

Gurnett, D. A., W. S. Kurth, G. B. Hospodarsky, A. M. Persoon, P. Zarka, A. Lecacheux, S. J. Bolton, M. D. Desch, W. M. Farrell, M. L. Kaiser, H. P. Ladreiter, H. O. Rucker, P. Galopeau, P. Louarn, D. T. Young, W. R. Pryor, and M. K. Dougherty, Control of Jupiter's radio emission and aurorae by the solar wind, *Nature* **415**, 985–987, 2002.

Hall, D., P. Feldman, M. A. McGrath, and D. F. Strobel, The far-ultraviolet oxygen airglow of Europa and Ganymede, *ApJ* **499**, 475–481, 1998.

Harris, W. M., J. T. Clarke, M. A. McGrath, and G. E. Ballester, Analysis of jovian auroral H Lyman-α emission (1981–1990), *Icarus* **23**, 350–365, 1996.

Hendrix, A. R., C. A. Barth, and C. W. Hord, Io's patchy SO_2 atmosphere as measured by the *Galileo* ultraviolet spectrometer, *J. Geophys. Res.* **104**, 11 817–11 826, 1999.

Higgins, C. A., T. D. Carr, F. Reyes, W. B. Greenman, and G. R. Lebo, A redefinition of Jupiter's rotation period, *J. Geophys. Res.* **102**, 22 033–22 041, 1997.

Hill, T. W., Inertial limit on corotation, *J. Geophys. Res.* **84**, 6554–6558, 1979.

Hill, T. W., The jovian auroral oval, *J. Geophys. Res.* **106**, 8101–8107, 2001.

Hill, T. W. and A. J. Dessler, Jupiter's magnetosphere, *Earth in Space* **8**, 6, 1995.

Hill, T. W. and V. M. Vasyliunas, jovian auroral signature of Io's corotational wake, *J. Geophys. Res.* **107**, 1462, 2002.

Hill, T. W., A. J. Dessler, and C. K. Goertz, Magnetospheric models, in *Physics of the jovian Magnetosphere*, A. J. Dessler (ed.), Cambridge University Press, pp. 353–394, 1983.

Hinson, D. P., A. J. Kliore, F. M. Flaser, J. D. Twicken, P. J. Schindler, and R. G. Herrera, *Galileo* radio occultation measurements of Io's ionosphere and plasma wake, *J. Geophys. Res.* **103**, 29 343–29 357, 1998.

Hospodarsky, G. B., I. W. Christopher, J. D. Menietti, W. S. Kurth, D. A. Gurnett, T. F. Averkamp, J. B. Groene, and P. Zarka, Control of jovian radio emissions by the Galilean moons as observed by *Cassini* and *Galileo*, in *Planetary Radio Emissions V*, H. O. Rucker, M. L. Kaiser and Y. Leblanc, eds, pp. 155–164, Austrian Academy of Sciences Press, 2001.

Huang, T. and T. Hill, Corotation lag of the jovian atmosphere, ionosphere and magnetosphere, *J. Geophys. Res.* **94**, 3761, 1984.

Huddleston, D. E., C. T. Russell, and G. Le, Magnetopause structure and the role of reconnection at the outer planets, *J. Geophys. Res.* **102**, 24 289–24 302, 1997.

Ingersoll, A. P. *et al.*, Imaging Jupiter's aurora at visible wavelengths, *Icarus* **135**, 251–264, 1998.

Isbell, J., A. J. Dessler, and J. H. Waite Jr., Magnetospheric energisation by interaction between planetary spin and the solar wind, *J. Geophys. Res.* **89**, 10 716–10 722, 1984.

Kaiser, M. L., Jovian and terrestrial low-frequency radio bursts: Possible cause of anomalous continuum, *J. Geophys. Res.* **103**, 19 993–20 000, 1998.

Kaiser, M. L., P. Zarka, W. S. Kurth, G. B. Hospodarsky, and D. A. Gurnett, *Cassini* and *Wind* stereoscopic observations of jovian non-thermal radio emissions: Measurements of beamwidths, *J. Geophys. Res.* **105**, 16 053–16 062, 2000.

Kennel, C. F. and F. V. Coroniti, Is Jupiter's magnetosphere like a pulsar's or Earth's?, in *The Magnetospheres of Earth and Jupiter*, V. Formisano (ed.), Reidel, p. 451, 1975.

Khurana, K. K., Euler potential models of Jupiter's magnetospheric field, *J. Geophys. Res.* **102**, 11 295–11 306, 1997.

Khurana, K. K., Influence of solar wind on Jupiter's magnetosphere deduced from currents in the equatorial plane, *J. Geophys. Res.* **106**, 25 999–26 016, 2001.

Khurana, K. K. and M. G. Kivelson, Inference of the angular velocity of plasma in the jovian magnetosphere from the sweepback of magnetic field, *J. Geophys. Res.* **98**, 67–79, 1993.

Kim, H. and J. L. Fox, The chemistry of hydrocarbon ions in the jovian ionosphere, *Icarus* **112**, 310–325, 1994.

Kim, Y. H., J. L. Fox, and H. S. Porter, Densities and vibrational distribution of H_3^+ in the jovian auroral ionosphere, *J. Geophys. Res.* **97**, 6093–6101, 1991.

Kim, Y. H., S. J. Kim, J. A. Stuewe, J. Caldwell, and T. M. Herbst, Jovian auroral ovals inferred from infrared H_3^+ images, *Icarus* **112**, 326–336, 1994.

Kim, Y. H., J. Caldwell, and J. Fox, High-resolution ultraviolet spectroscopy of Jupiter's aurora with the Hubble Space Telescope, *ApJ* **447**, 906–914, 1995.

Kivelson, M. G., K. K. Khurana, C. T. Russell, R. J. Walker, J. Warnecke, F. V. Coroniti, C. Polanskey, D. J. Southwood, and C. Schubert, Discovery of Ganymede's magnetic field by the *Galileo* spacecraft, *Nature* **384**, 537–541, 1996.

Kliore, A., D. L. Cain, G. Fjeldbo, B. L. Seidel, and S. I. Rasool, Preliminary results on the atmospheres of Io and Jupiter from the *Pioneer 10* S–band occultation experiment, *Science* **183**, 323–324, 1974.

Knight, S., Parallel electric fields, *Planet. Space Sci.* **21**, 741–750, 1973.

Kostiuk, T., P. N. Romani, F. Espenak, T. A. Livengood, and J. J. Goldstein, Temperature and abundances in the jovian auroral stratosphere: 2. Ethylene as a probe of the microbar region, *J. Geophys. Res.* **98**, 18 823–18 830, 1993.

Kurth, W., D. A. Gurnett, and J. D. Menietti, The influence of the Galilean satellites on radio emissions from the jovian system, in *Radio Astronomy at Long Wavelengths*, G.R. Stone, AGU Monograph 119, pp. 213–217, 2000.

Kurth, W. S., Continuum radiation in planetary magnetospheres, in *Planetary Radio Emissions III*, H. O. Rucker, M. L. Kaiser,

and Y. Leblanc, eds, pp. 329–350, Austrian Academy of Sciences Press, 1992.

Ladreiter, H. P., P. Zarka, and A. Lecacheux, Direction finding study of jovian hectometric and broadband kilometric radio emissions: Evidence for their auroral origin, *Planet. Space Sci.* **42**, 919–931, 1994.

Le Quéau, D., Planetary radio emissions from high magnetic latitudes: The "cyclotron maser" theory, in *Planetary Radio Emissions II*, H. O. Rucker, M. L. Kaiser, and Y. Leblanc, eds, pp. 381–398, Austrian Academy of Sciences Press, Vienna, 1988.

Lepping, R. P., M. D. Desch, L. W. Klein, E. C. Sittler Jr., J. D. Sullivan, W. S. Kurth, and K. W. Behannon, Structure and other properties of Jupiter's distant magnetotail, *J. Geophys. Res.* **88**, 8801–8815, 1983.

Liu, W. and A. Dalgarno, The ultraviolet spectra of the jovian aurora, *ApJ* **467**, 446–453, 1996.

Livengood, T. A., H. W. Moos, G. E. Ballester, and R. M. Prangé, Jovian ultraviolet auroral activity, *Icarus* **97**, 26–45, 1992.

Livengood, T. A., T. Kostiuk, F. Espenak, and J. J. Goldstein, Temperature and abundances in the jovian auroral stratosphere: 1. Ethane as a probe of the millibar region, *J. Geophys. Res.* **98**, 18 813–18 822, 1993.

Louarn, P., Auroral planetary radio emissions: Theoretical aspects, *Adv. Space Res.* **12**, 121–134, 1992.

Louarn, P., A. Roux, S. Perraut, W. Kurth, and D. Gurnett, A study of the large-scale dynamics of the jovian magnetosphere using the *Galileo* plasma wave experiment, *Geophys. Res. Lett.* **25**, 2905–2908, 1998.

MacDowall, R. J., M. L. Kaiser, M. D. Desch, W. M. Farell, R. A. Hess, and R. G. Stone, Quasi-periodic jovian radio bursts: Observations from the *Ulysses* radio and plasma wave experiment, *Planet. Space Sci.* **41**, 1059–1072, 1993.

Mauk, B. H., J. T. Clarke, D. Grodent, J. H. Waite Jr., C. P. Paranicas, and D. J. Williams, Transient aurora at Jupiter from injections of magnetospheric electrons: A pulsating auroral x-ray hot spot on Jupiter, *Nature* **415**, 1003–1005, 2002.

Maurellis, A. N., T. E. Cravens, G. R. Gladstone, J. H. Waite, and L. W. Acton, Jovian x-ray emission from solar x-ray scattering, *Geophys. Res. Lett.* **27**, 1339–1342, 2000.

Metzger, A. E., D. A. Gilman, J. L. Luthey, K. C. Hurley, H. W. Schnopper, F. D. Seward, and J. D. Sullivan, The detection of x rays from Jupiter, *J. Geophys. Res.* **88**, 7731–7741, 1983.

Miller, S., D. Rego, N. Achilleos, T. S. Stallard, R. Prangé, M. Dougherty, R. D. Joseph, J. Tennyson, A. Aylward, I. Meuller-Wodarg, and D. Rees, Infrared spectroscopic studies of the jovian ionosphere and aurorae, *Adv. Space Res.* **26**, 1477–1488, 2000.

Morrissey, P. F., P. D. Feldman, J. T. Clarke, B. C. Wolfven, D. F. Strobel, S. T. Durrance, and J. T. Trauger, Simultaneous spectroscopy and imaging of the jovian aurora with the Hopkins Ultraviolet Telescope and the Hubble Space Telescope, *ApJ* **476**, 918–923, 1997.

Neubauer, F. M., Nonlinear standing Alfvén wave current system at Io: Theory, *J. Geophys. Res.* **85**, 1171–1178, 1980.

Pallier, L. and R. Prangé, More about the structure of the high latitude jovian aurorae, *Planet. Space Sci.* **49**, 1159–1173, 2001.

Paschmann, G., S. Haaland, and R. Treuman, Auroral plasma physics, *Space Sci. Rev.* **103**, 1–475, 2002.

Piddington, J. and D. Drake, Electrodynamics effects of Jupiter's satellite Io, *Nature* **217**, 935, 1968.

Pontius Jr., D. H., Radial mass transport and rotational dynamics, *J. Geophys. Res.* **102**, 7137–7150, 1997.

Prangé, R., P. Zarka, G. E. Ballester, T. A. Livengood, L. Denis, T. Carr, F. Reyes, S. J. Bame, and H. W. Moos, Correlated variations of UV and radio emissions during an outstanding jovian auroral event, *J. Geophys. Res.* **98**, 18 779–18 791, 1993.

Prangé, R., I. M. Engle, J. T. Clarke, M. Dunlop, G. E. Ballester, W. H. Ip, S. Maurice, and J. Trauger, Auroral signature of Comet Shoemaker–Levy–9 in the jovian magnetosphere, *Science* **267**, 1317–1320, 1995.

Prangé, R., D. Rego, D. Southwood, P. Zarka, S. Miller, and W.-H. Ip, Rapid energy dissipation and variability of the Io–Jupiter electrodynamic circuit, *Nature* **379**, 323–325, 1996.

Prangé, R., D. Rego, L. Pallier, J. E. P. Connerney, P. Zarka, and J. Queinnec, Detailed study of FUV jovian auroral features with the post-COSTAR HST Faint Object Camera, *J. Geophys. Res.* **103**, 20 195–20 216, 1998.

Prangé, R., G. Chagnon, M. G. Kivelson, T. A. Livengood, and W. S. Kurth, Temporal monitoring of Jupiter's auroral activity with IUE during the *Galileo* mission: Implications for magnetospheric processes, *Planet. Space Sci.* **49**, 405–415, 2001.

Queinnec, J. and P. Zarka, Io–controlled decameter arcs and Io–Jupiter interaction, *J. Geophys. Res.* **103**, 26 649–26 666, 1998.

Queinnec, J. and P. Zarka, Flux, power, energy and polarization of jovian S-bursts, *Planet. Space Sci.* **49**, 365–376, 2001.

Rego, D., R. Prangé, and L. B. Jaffel, Lyman-α and H_2 bands from the giant planets: 3. Intensity and spectral profile of the auroral lyman-α emission, including charge exchange and radiative transfer effects, *J. Geophys. Res.* **104**, 5939–5954, 1999a.

Rego, D., N. Achilleos, T. Stallard, S. Miller, R. Prangé, M. Dougherty, and R. Joseph, Supersonic winds in Jupiter's aurorae, *Nature* **399**, 121–124, 1999b.

Reiner, M. J., J. Fainberg, R. G. Stone, M. L. Kaiser, M. D. Desch, R. Manning, P. Zarka, and B. M. Pedersen, Source characteristics of jovian narrow-band kilometric radio emissions, *J. Geophys. Res.* **98**, 13 163–13 176, 1993.

Retherford, K. D., H. W. Moos, D. F. Strobel, B. C. Wolven, and F. L. Roesler, Io's equatorial spots: Morphology of neutral UV emissions, *J. Geophys. Res.* **105**, 27 157–27 165, 2000.

Roesler, F. L., H. W. Moos, R. J. Oliversen, R. C. Woodward, K. D. Retherford, F. Scherb, M. A. McGrath, W. H. Smyth, P. D. Feldman, and D. F. Strobel, Far-ultraviolet imaging spectroscopy of Io's atmosphere with HST STIS, *Science* **283**, 353–357, 1999.

Russell, C. T., Z. J. Yu, K. K. Khurana, and M. G. Kivelson, Magnetic field changes in the inner magnetosphere of Jupiter, *Adv. Space Res.* **28**, 897–902, 2001.

Sandel, B. R., D. E. Shemansky, A. L. Broadfoot, J. L. Bertaux, J. E. Blamont, M. J. S. Belton, J. M. Ajello, J. B. Holberg, S. K. Atreya, T. M. Donahue, H. W. Moos, D. F. Strobel, J. C. McConnell, A. Dalgarno, R. Goody, M. B. McElroy, and P. Z. Takacs, Extreme ultraviolet observations from *Voyager 2* encounter with Jupiter, *Science* **206**, 962–966, 1979.

Satoh, T. and J. E. P. Connerney, Jupiter's H_3^+ emissions viewed in corrected jovimagnetic coordinates, *Icarus* **141**, 253–262, 1999.

Satoh, T., J. E. P. Connerney, and R. Baron, Emission source model of Jupiter's H_3^+ aurorae: A generalized inverse analysis of images, *Icarus* **122**, 1–23, 1996.

Saur, J., F. M. Neubauer, D. F. Strobel, and M. E. Summers, Three dimensional plasma simulation of Io's interaction with the Io plasma torus, *J. Geophys. Res.* **104**, 25 105–25 126, 1999.

Saur, J., A. Pouquet, and W. H. Matthaeus, An acceleration mechanism for the generation of the main auroral oval on Jupiter, *Geophys. Res. Lett.* **30**, 1260, 2003.

Scudder, J. D., E. C. Sittler Jr., and H. S. Bridge, A survey of the plasma electron environment of Jupiter: A view from *Voyager*, *J. Geophys. Res.* **86**, 8157–8179, 1981.

Shaposhnikov, V. E., V. V. Zaitsev, H. O. Rucker, and G. V. Litvinenko, Origin of ultraviolet emission source in the jovian ionosphere at the feet of the Io flux tube, *J. Geophys. Res.* **106**, 26 049–26 056, 2001.

Skinner, T. E. and H. W. Moos, Comparison of the jovian north and south pole aurorae using the IUE observatory, *Geophys. Res. Lett.* **11**, 1107–1110, 1984.

Southwood, D. J. and M. G. Kivelson, A new perspective concerning the influence of the solar wind on Jupiter, *J. Geophys. Res.* **106**, 6123–6130, 2001.

Stallard, T. S., S. Miller, G. Millward, and R. D. Joseph, On the dynamics of the jovian ionosphere and thermosphere: 1. The measurement of ion winds, *Icarus* **154**, 475–491, 2001.

Stallard, T. S., S. Miller, S. W. H. Cowley, and E. J. Bunce, Jupiter's polar ionospheric flows: Measured intensity and velocity variations poleward of the main auroral oval, *Geophys. Res. Lett.* **30**, 1221, 2003.

Su, Y.-J., R. Ergun, F. Bagenal, and P. Delamere, Io-related jovian auroral arcs: Modeling parallel electric fields, *J. Geophys. Res.* **108**, 1094, 2003.

Thorne, R. M., Microscopic plasma processes in the jovian magnetosphere, in *Physics of the Jovian Magnetosphere*, A. J. Dessler (ed.), Cambridge University Press, 1983.

Trafton, L., D. F. Lester, and K. L. Thompson, Unidentified emission lines in Jupiter's northern and southern 2 μm aurorae, *ApJ* **343**, L73–L76, 1989.

Trafton, L., J.-C. Gérard, G. Munhoven, and H. Waite, High–resolution spectra of Jupiter's northern auroral ultraviolet emission with the Hubble Space Telescope, *ApJ* **421**, 816–827, 1994.

Trauger, J. T., J. T. Clarke, G. E. Ballester, R. W. Evans, C. J. Burrows, D. Crisp, I. Gallagher, J. S., R. E. Griffiths, J. J. Hester, J. G. Hoessel, J. A. Holtzmann, J. E. Krist, J. R. Mould, R. Sahai, P. A. Scowen, K. R. Stapelfeldt, and A. M. Watson, Saturn's hydrogen aurora: Wide Field and Planetary Camera 2 imaging from the Hubble Space Telescope, *J. Geophys. Res.* **103**, 20 237–20 244, 1998.

Tsurutani, B. T., J. K. Arbello, B. E. Goldstein, C. M. Ho, G. S. Lakhina, E. J. Smith, N. Cornilleau-Wherlin, R. Prangé, N. Lin, P. Kellogg, J. L. Philips, A. Balogh, N. Krupp, and M. Kane, Plasma wave characteristics of the jovian magnetopause boundary layer: Relationship to the jovian aurora?, *J. Geophys. Res.* **102**, 4751–4764, 1997.

Vasavada, A. R. and *et al.*, Jupiter's visible aurora and Io footprint, *J. Geophys. Res.* **104**, 27 133–27 142, 1999.

Vasyliūnas, V. M., Plasma distribution and flow, in *Physics of the Jovian Magnetosphere*, A. J. Dessler (ed.), Cambridge University Press, pp. 395–453, 1983.

Waite Jr., J. H., T. E. Cravens, J. Kozyra, A. F. Nagy, S. K. Atreya, and R. H. Chen, Electron precipitation and related aeronomy of the jovian thermosphere and ionosphere, *J. Geophys. Res.* **88**, 6143–6163, 1983.

Waite Jr., J. H., J. T. Clarke, and T. Cravens, The jovian aurora: Electron or ion precipitation?, *J. Geophys. Res.* **93**, 7244–7250, 1988.

Waite Jr., J. H., F. Bagenal, F. Seward, C. Na, G. R. Gladstone, T. E. Cravens, K. C. Hurley, J. T. Clarke, R. Elsner, and S. A. Stern, ROSAT observations of the Jupiter aurora, *J. Geophys. Res.* **99**, 14 799–14 809, 1994.

Waite Jr., J. H., D. Grodent, G. R. Gladstone, S. J. Bolton, J. T. Clarke, J.-C. Gérard, W. S. Lewis, L. M. Trafton, A. P. Ingersoll, and J. E. P. Connerney, Multispectral observations of Jupiter's aurora, *Adv. Space Res.* **26**, 1453–1475, 2000.

Waite Jr., J. H., G. R. Gladstone, W. S. Lewis, R. Goldstein, D. J. McComas, P. Riley, R. J. Walker, P. Robertson, S. Desai, J. T. Clarke, and D. T. Young, An auroral flare at Jupiter, *Nature* **410**, 787–789, 2001.

Walker Jr., J. H. and C. T. Russell, Flux transfer events at the jovian magnetopause, *J. Geophys. Res.* **90**, 7397–7405, 1985.

Warwick, J. W., J. B. Pearce, R. G. Peltzer, and A. C. Riddle, Planetary radio astronomy experiment for the *Voyager* missions, *Space Sci. Rev.* **21**, 309, 1977.

Williams, D. J., R. M. Thorne, and B. Mauk, Energetic electron beams and trapped electrons at Io, *J. Geophys. Res.* **104**, 14 739–14 754, 1999.

Woch, J., N. Krupp, and A. Lagg, Particle burst in the jovian magnetosphere: Evidence for a near-Jupiter neutral line, *Geophys. Res. Lett.* **29**, 10.1027, 2002.

Wolven, B. C. and P. D. Feldman, Self-absorption by vibrationally excited H_2 in the *Astro-2* Hopkins Ultraviolet Telescope spectrum of the jovian aurora, *Geophys. Res. Lett.* **25**, 1537, 1998.

Yung, Y. L., G. R. Gladstone, K. M. Chang, J. M. Ajello, and S. K. Srivastava, H_2 fluorescence from 1200 to 1700 A by electron impact: Laboratory study and application to jovian aurora, *ApJ* **254**, L65–L69, 1982.

Zarka, P., Auroral radio emissions at the outer planets: Observations and theories, *J. Geophys. Res.* **103**, 20 159–20 194, 1998.

Zarka, P., Radio emissions from the planets and their moons, in *Radio Astronomy at Long Wavelengths*, G. R. Stone (ed.), AGU, pp. 167–178, 2000.

Zarka, P., T. Farges, B. P. Ryabov, M. Abada-Simon, and L. Denis, A scenario for jovian S-bursts, *Geophys. Res. Lett.* **23**, 125–128, 1996.

Zarka, P., J. Queinnec, and F. Crary, Low-frequency limit of jovian radio emissions and implications on source locations and Io plasma wake, *Planet. Space Rev.* **49**, 1137–1149, 2001a.

Zarka, P., R. A. Treumann, B. P. Ryabov, and V. B. Ryabov, Magnetically-driven planetary radio emissions and applications to extrasolar planets, *Astrophys. Space Sci.* **277**, 293–300, 2001b.